C.P. No. 1309

C.P. No. 1309

PROCUREMENT EXECUTIVE, MINISTRY OF DEFENCE

AERONAUTICAL RESEARCH COUNCIL

CURRENT PAPERS

The Prediction of Boundary-Layer Behaviour and Profile Drag for Infinite Yawed Wings: Part III Calculations for a Particular Wing

by

B. G. J. Thompson, G. A. Carr-Hill and M. Ralph

Aerodynamics Dept., R.A.E., Teddington

LONDON: HER MAJESTY'S STATIONERY OFFICE

1974

PRICE £1 - 35 NET

UDC 533.693.1 : 532.526 : 533.6.048.3 : 533.6.013.122 : 533.6.013.154

* CP No.1309

May 1973

THE PREDICTION OF BOUNDARY-LAYER BEHAVIOUR AND PROFILE DRAG FOR INFINITE YAWED WINGS PART III: CALCULATIONS FOR A PARTICULAR WING

by

B. G. J. Thompson**

G. A. Carr-Hill

M. Ralph

SUMMARY

An integral method is used to predict boundary-layer and wake behaviour for a family of infinite yawed wings having a chordwise section NPL 3111 operating at its design sonic rooftop condition.

Profile drag predictions show a smaller variation with yaw than a typical project office design method. The Reynolds number for incipient rear separation depends strongly on angle of yaw. Scale effect on loss of lift, due to viscous displacement of the potential flow, appears to be amplified by sweep.

---

* Replaces RAE Technical Report 73090 - ARC 35094.

** Now with the DOE, CEDAR project, PCAO (DBD), Lunar House, Croydon.

solution is found using the method of Nath[8]. Some predictions for flow on swept leading edges in compressible flow are presented in Ref.5.

The turbulent layer is calculated using the integral entrainment method of Cumpsty and Head[9-12] together with the compressibility assumptions of Green[13], but the equations for the integral quantities are not solved by using the global iteration scheme of Ref.9, for the reasons given by Thompson and Macdonald[4].

Transition and wake assumptions were chosen to be compatible with the Nash drag prediction procedure[14] in two dimensions. The extension to infinite yawed wing conditions was made in a manner that followed closely the approach of Cooke[2].

The results for profile drag are discussed in section 4.1 and are compared with predictions (of the type used in project design) employing sweep factors, as suggested by Rossiter[3], with the skin-friction relationships of Ref.29. The following sections then consider displacement effect and rear separation, neither of which could be found from the simpler methods which are currently in use at the project design stage.

At the smaller sweep angles and Reynolds numbers, the results depend upon the assumptions for transition behaviour, especially upon the assumed 'transition point'. The sensitivity of profile drag to transition position is compared with the effect of sweep in section 4.1.

Simple project studies for a variable sweep wing, operating at the above section design conditions, are then considered in Appendix A, and the Report concludes with two additional Appendices. The first of these examines rigorously the conditions for which section properties in inviscid potential flow are independent of sweep, whilst the second considers further the basic assumptions underlying the use of sweep and form factors for profile drag determination.

Since the present parametric study was started, a more sophisticated method[20] of predicting the turbulent boundary layer on infinite yawed wings has been published. However, because of the limitations of the numerical method in that paper, this cannot yet be started at the attachment line and is also much slower than an integral procedure. It is suitable for spot checks only, therefore, using the present method to start it off. The biggest problem is, however, that Bradshaw's equations are programmed only for incompressible flow and cannot be used in their present form to make comparisons with the results obtained here for a realistic range of transonic conditions.

2 THE METHOD OF CALCULATION

The complete calculation procedure, as described fully in Ref.4, consists of a laminar boundary-layer calculation, an assumed transition behaviour at an input transition position, followed by the turbulent boundary-layer prediction. A simple wake relationship is then used to relate the trailing-edge properties to the conditions at infinity downstream in order to yield a value of profile drag. An extension of the work of Cumpsty and Head[10], to compressible flow, is used if the attachment line flow is fully turbulent. These features are summarized below.

Ref.4 also presents details of the numerical methods of handling input data (smoothing, interpolation and differentiation of freestream velocities, for example) and considers methods of solving the boundary-layer integral equations. For potential users computing details are given, especially the relationships between computing time, step length and accuracy.

2.1 The compressible flow along the swept leading-edge attachment line

The parameter that characterises the attachment line flow and hence the changeover from laminar to turbulent flow there, is

$$C^* = \frac{U_\infty^2 \sin^2 \Lambda}{\nu_{a.l.} \left[dU_l/ds'\right]_{a.l.}} \quad , \tag{1}$$

as first defined by Cumpsty and Head[10]. Their experiments in incompressible flow showed that, for a fully turbulent attachment line boundary layer to exist, the value of C^* must be at least 7×10^4 and that a value of 1.2×10^5 may be required. The lower figure has been taken for the present work, and has been assumed[4] to hold for compressible flow in the range,

$$0 \leqslant M_{a.l.} \leqslant 2 \quad .$$

Analytical approximations to the variations of H, $R_{\theta_{11}}$ and $\theta_{11}\partial\beta/\partial s'$ with C^* and $M_{a.l.}$ are given in Ref.4 and, by assuming a simple expansion in terms of surface distance chordwise, the initial values for a turbulent boundary-layer calculation can be obtained.

2.2 The laminar boundary layer

If the flow along the attachment line is laminar, then the compressible laminar boundary layer is computed assuming the 'independence principle'[18] to hold approximately[4]. That is, a solution of the chordwise integral momentum equation is obtained using Thwaites' method[6], whilst the spanwise momentum equation is solved separately using Nath's procedure[8], assuming a universal velocity profile shape in the spanwise direction. In each case the Rott[7] transformation is applied to allow for the effects of compressibility.

2.3 Transition

Across any assumed transition front, Cooke[22] showed that the components of momentum defect in the chordwise and spanwise directions must remain unchanged. This requirement provides two relationships, but in order to start the turbulent boundary-layer calculation a third condition is required. For simplicity and for consistency with the work of Nash *et al.*[14] on the prediction of profile drag in two-dimensions, it was assumed that the shape-factor (G) of the streamwise velocity profile took its local equilibrium value at the start of the turbulent flow. An iterative numerical scheme then allowed values of streamwise H_1, θ_{11}/c' and $\tan\beta$ to be calculated.

The restrictive nature, both of the spanwise laminar velocity profile (a Blasius flat plate profile is assumed) and of the turbulent cross-flow profile (Mager's assumptions[30] together with power-law profiles streamwise are used) lead, in favourable pressure gradients, to a slight rise at transition in the value of surface streamline angle β_t, as Fig.13 shows. This is not realistic, but the error is likely to be very small, as the angles (β_ℓ and β_t) are small. The cross-flow angle β_t is much less than the laminar value in adverse pressure gradients ($x'_{tr}/c' = 0.36$). This is in accordance with experimental observations[24] which suggest that the cross-flow angle falls to a very small value just after transition has taken place.

2.4 The turbulent boundary layer

The equations[32,4] for streamwise momentum and cross-flow momentum development in compressible flow are solved simultaneously with the entrainment integral equation[33,4] after casting them in terms of the three independent variables $\tan\beta$, $(\delta - \delta^*)/c'$, and θ_{11}/c'. The global iteration method of solution given in Ref.9 is shown in Ref.4 to fail in regions of favourable

pressure gradient just downstream of a turbulent attachment line and so was discarded in favour of a simple step-by-step method.

Additional assumptions are required for entrainment rate (F), streamwise and chordwise velocity profile shapes, and streamwise skin-friction. These relations are summarized here as follows:

(a) Entrainment

$$F = F(H_1) = 0.0299(H_1 - 3)^{-0.617} \tag{2}$$

from Thompson[34].

(b) Streamwise profiles are related by two one-parameter expressions depending upon the local Mach number. That is, if $M_e \leq 0.3$, the analytic approximations for streamwise shape factor for incompressible flow given by Thompson[35] are used. If $M_e > 0.3$ then a better approximation is suggested by Green[36], namely, for $H_1 \geq 3.74$ (at which value separation is assumed to occur),

$$\bar{H} = 1 + 1.12\left(H_1 - 2 - \sqrt{(H_1 - 2)^2 - 3}\right)^{0.915} \tag{3}$$

with $\bar{H}$ being taken as the analogue of the incompressible H. For compressible flow we have,

$$H = \left(1 + 0.2M_e^2\right)\bar{H} + 0.2rM_e^2 \tag{4}$$

if the recovery factor, $r = 0.89$.

(c) In order to evaluate integrals depending wholly or partly upon the cross-flow profile, the compressibility transformation

$$d\eta = (\rho/\rho_e)dz/\bar{\delta} \ , \tag{5}$$

where

$$\bar{\delta} = \int_0^{\delta} \rho/\rho_e dz \ , \tag{6}$$

was assumed, following Green[13]. Then by using the power law profiles,

$$\frac{u}{U_e} = \eta^n , \qquad n = \frac{\bar{H} - 1}{2} , \tag{7}$$

and the cross-flow assumption due to Mager[30], in the form,

$$\frac{v}{U_e} = (1 - \eta)^2 \eta^n \tan \beta , \tag{8}$$

all required properties can be evaluated.

(d) The component $\left(c_{f_l}\right)$ of skin-friction in the direction of the local freestream velocity vector is assumed to be given by the relationship for two-dimensional flow due to Green[36]. This was based to some extent on his own compressible flow data[37] and is cast in the form used by Spalding and Chi[38]. However, in the present work, the functions F_r, F_c are analytically approximated as suggested by Nash *et al.*[31]. That is,

$$c_{f_l} = c_{f_{plate}} \left[\frac{0.9}{\left(\bar{H}/\bar{H}_{plate} - 0.4 \right)} - 0.5 \right] , \tag{9}$$

$$\bar{H}_{plate} = \left(1 - 6.8 \sqrt{\frac{c_{f_{plate}}}{2}} \right)^{-1} , \tag{10}$$

$$c_{f_{plate}} = \frac{1}{F_c} \left[\frac{0.012}{\left(\log_{10} \left(F_r R_{\theta_{11}} \right) - 0.64 \right)} - 0.00093 \right] , \tag{11}$$

$$F_r = 1 - 0.134 M_e^2 + 0.027 M_e^3 , \tag{12}$$

$$F_c = \left(1 + 0.066 M_e^2 - 0.008 M_e^3 \right)^2 . \tag{13}$$

2.5 Separation

Separation occurs (strictly) when the predicted surface streamlines become parallel to the generators of the infinite wing; that is, when,

$$\beta + \phi = 90^{o} \quad ,$$

or equivalently, $c_{f_{x'}} = 0$.

Because of the need to define separation boundaries and (hopefully) to predict the initial drag increase that might occur with very small amounts of rear separation, the turbulent boundary-layer predictions are continued beyond separation if this occurs for $x'/c' \gtrsim 0.9$, by setting

$$\tan \beta = \frac{0.999}{\tan \phi} \quad , \tag{14}$$

if the calculated value of $\tan \beta$ is greater than that quantity.

c_{f_1} is limited to not less than 10^{-6}, and H_1, $\bar{H}$ and hence F also are constrained at their separation values.

2.6 The wake in infinite yawed flow and the prediction of the profile drag value

The procedure suggested by Cooke[2] is followed except that the flow in the chordwise plane is assumed to follow the relationship proposed for compressible two-dimensional flow by Nash, and reported in Ref.39.

Hence we have

$$\theta'_{\infty} = \theta'_{t.e.} \left[\frac{\left(T_e\right)_{t.e.}}{T_{\infty}} \right]^{3} \left[\frac{\left(U_e \cos \phi\right)_{t.e.}}{U_{\infty} \cos \Lambda} \right]^{\chi} \quad ,$$

where

$$\chi = 0.28571(1 + H'_{t.e.}) \frac{T_{\infty}}{T_0} + 2.4286 \quad . \tag{15}$$

Taking spanwise components to be denoted by the superscript s we have

$$\theta^{s}_{\infty} = \theta^{s}_{t.e.} \left[\frac{\left(U_e\right)_{t.e.}}{U_{\infty}} \right]^{2} \left[\frac{\left(T_e\right)_{t.e.}}{T_{\infty}} \right]^{2.5} \quad , \tag{16}$$

and

$$C_D = 2\left(\theta'_\infty \cos^3 \Lambda + \theta^s_\infty \sin \Lambda\right) \quad , \tag{17}$$

where, in terms of conventional streamwise and cross-flow profile parameters:

$$\theta' = \theta_{11} - \tan\phi\,(\theta_{21} + \theta_{12}) + \theta_{22} \tan^2 \phi \quad , \tag{18}$$

$$\theta^s = \cos^2 \phi \left\{\tan\phi\,(\theta_{11} - \theta_{22}) + \theta_{21} - \theta_{12} \tan^2 \phi\right\} \quad , \tag{19}$$

and

$$H' = \left(\delta^*_1 - \delta^*_2 \tan\phi\right) \Big/ \theta' \quad . \tag{20}$$

3 THE EFFECTS OF YAW

3.1 The basis of the parametric study

Fig.1a explains concisely most of the notation used in discussing infinite yawed wings.

The distribution of $C_p \sec^2 \Lambda$ used as input for the present computations is shown in Fig.2. The velocity component normal to the leading edge is plotted in Fig.3 for the stagnation region, and this shows how the value of 'effective' leading-edge radius was arrived at using the velocity gradient at the attachment line. The pressures used were taken from the measurements of Firmin and Cook[17].

The section properties are

$$C_L \sec^2 \Lambda = 0.515 \quad ,$$

$$M_\infty \cos \Lambda = 0.665 \quad . \tag{21}$$

The corresponding variations of true C_L and M_∞ with Λ are given in Fig.4.

In the present calculations, the relevant range of conditions is $0^\circ \leqslant \Lambda \leqslant 60^\circ$, corresponding to values of the attachment line Mach number, $M_{a.l.}$ in the range

$$0 \leqslant M_{a.l.} \leqslant 1.15 \quad , \tag{22}$$

and the compressibility assumptions with regard to the attachment line flow should be quite adequate over this modest range (*cf.* section 3.1 above).

Figs.11a and 11b show, in the plane $\log_{10} R_c$ *versus* Λ, the curve $C^* = 7 \times 10^4$, for the 'effective' attachment line radius $\sigma'/c' = 0.0235$ appropriate to NPL 3111*.

'Boxes' are shown to indicate the approximate cruise conditions for typical modern subsonic transport aircraft such as the Lockheed C 5-A, and the A-300 Airbus and BAC 311 projects. If these machines have sections with leading-edge conditions similar to those of Fig.3, then they will cruise with marginally turbulent flow at the leading edge.

3.2 Results of the present calculations

Typical external streamline shapes are shown for the upper surface only in Fig.5, for $\Lambda = 20^\circ$, and 40°. This gives some idea of the degree of fuselage or wind tunnel wall shaping necessary to cancel out end effects. Corresponding surface streamlines are plotted for a streamwise chord Reynolds number (R_c) of 2×10^7. The flow is fully turbulent across the complete chord at $\Lambda = 40^\circ$, but not at $\Lambda = 20^\circ$, where the effect of different transition positions is seen.

Some corresponding displacement thickness developments are given in Fig.8, whilst, in Fig.12, the variation of chordwise component $\left(c_{f_{x'}}\right)$ of skin-friction is shown in conditions ($R_{c'} = 10^7$) which are more appropriate to a discussion of the separation boundaries at small angles of sweep.

For layers turbulent from the leading edge**, the above conditions $\left(R_{c'} = 10^7\right)$ lead to a trailing-edge separation at roughly 35° sweep (Fig.11b).

The remaining figures show the results of the parametric study for behaviour of profile drag in Figs.6 and 7, rear separation (in Figs.11a and b), and of displacement effect at the trailing edge (in Figs.9 and 10). These results are described and discussed in sections 5.1 to 5.3, whilst cross-flow

---

* True geometric attachment line radius is 0.011c for this section.

** To avoid tedious repetition, this and similar looser phrases like 'full-chord turbulent flow' are used throughout the present text to mean, "if laminar at the attachment line then transition was taken for convenience at $x'_{tr}/c' = 0.0155$ on both surfaces, otherwise the flow was turbulent at the attachment line".

and the transition assumptions are considered further using Figs.13 and 14. To conclude, a simple project exercise was carried out for an idealised variable sweep wing (see Figs.15, 16 and 17) and this exercise is described in Appendix A.

3.3 Computing details

Approximately 220 boundary-layer calculations were involved using, for the turbulent layer, step lengths along the local external streamlines, of ten boundary-layer thicknesses or 0.01c whichever was the smaller. An average of 40 seconds of KDF9 time was required for each calculation including extensive print out. A full description of the numerical method and details of the relationship between computing time, step length etc., is provided in Ref.4.

4 DISCUSSION

4.1 Profile drag

For layers turbulent from the leading edge the results of the calculations are shown as a function of R_c and Λ, in Fig.6, where they are compared with the predictions obtained from the use of the sweep factor approach as suggested by Rossiter[3] using the skin-friction charts of Ref.29. The basic relationship of the latter method (see Appendix C for further details) is

$$C_{DP_{3\text{-}D}}(R_c,M_\infty) = C_{F_{plate}}(R_c,0)\left[\left\{\lambda_w - 1\right\}\cos^3\Lambda + 1\right] \quad , \qquad (C\text{-}7)$$

where the sectional form factor

$$\lambda_w = \lambda_w(M_\infty \cos\Lambda) = \frac{C_{DP_{2\text{-}D}}(R_c,M_\infty \cos\Lambda)}{C_{F_{plate}}(R_c,0)} \quad , \qquad (C\text{-}8)$$

and the values of $C_{DP_{2\text{-}D}}$ were obtained from the present calculation method in its two-dimensional form.

The difference between the two sets of predictions increases with sweep and the sweep factor method always gives the smaller values. The difference is about 2½% at $\Lambda = 30^\circ$. This may be regarded as small, considering the number of relatively crude assumptions inherent in either method.

Rear separation, which has been plotted here from the boundary-layer calculations and corresponds to the curve for $c_{f_{x'}} = 1 \times 10^{-6}$ at the trailing edge in Fig.11a, cannot be predicted using the sweep factor method (see section 4.3 below). The values of C_{DP} obtained by the present calculation method rise rapidly once rear separation has occurred (see Fig.6) but cannot be relied upon quantitatively (see Ref.4).

Profile drag depends not only upon the angle of yaw but also upon the location of transition. Fig.7 shows the relative sensitivity of upper surface drag (C_{DU}) to both of these factors, when $R_c = 2 \times 10^7$. It is seen that, for this 'rooftop' aerofoil, the same change in drag coefficient is produced by a 30° change of sweep with a given transition position as would be produced by a movement in transition of about 10% of chord with the angle of sweep held constant.

4.2 Displacement effect, with full chord turbulent flow

The distributions of displacement thickness shown in Fig.8 result in the alteration of the effective aerofoil mean lines as indicated in Fig.9. The relative changes of camber are shown by normalising on the values at the trailing edge. Since the interaction between the varying displacement surface shape and the surface pressures, (which would certainly become significant for the larger angles of yaw near separation) has not been calculated in the present work, only the changes of incidence $\Delta(\alpha, \sec \Lambda)$ are shown, in Fig.10, as a function of R_c and Λ.

At any given value of R_c, the loss of incidence rises with Λ until, at separation, it may be several times the value for the unyawed wing. For example, if a streamwise chord Reynolds number of 2×10^7 is considered once again, the loss of incidence is 0.172 degrees at $\Lambda = 0^\circ$, rising to 0.38 degrees at separation where $\Lambda = 38.5^\circ$. This additional effect of yaw is approximately independent of the value of R_c considered and can be taken as 0.2 degree.

Now, the lift-curve slope at $R_c = 15.6 \times 10^6$ was about 0.15 per degree in the two-dimensional tests[16]. Therefore, the maximum loss of $C_L \sec^2 \Lambda$, due to yaw, will be nearly 6% of the design value. This estimate is based solely upon the change in effective incidence; the camber changes will further reduce $C_L \sec^2 \Lambda$ but the increased total thickness of the displacement surface at higher values of Λ will raise the lift slightly. Hence the present estimates are probably satisfactory as a guide.

A fixed increment of R_c, for instance that relating a wind tunnel model to the corresponding flight conditions, results in a change of incidence due to scale effect that becomes larger with sweep. For example, considering for convenience here the range,

$$1.3 \times 10^7 \leq R_c \leq 2 \times 10^8 \quad ,$$

the change in $\Delta(\alpha \sec \Lambda)$ is 0.125 degree, in the unyawed state, rising to 0.185 degree at $\Lambda = 30^\circ$.

4.3 Rear separation

The streamwise chord Reynolds number, for which separation is imminent at the trailing edge, is shown in Figs.11a and b as a function of Λ.

Bearing in mind that any method based upon the boundary-layer approximation breaks down close to separation, and that qualitative experience in two-dimensions is the only guide, separation boundaries are plotted (in Fig.11a) for two (small) values of chordwise skin-friction component $\left(c_{f_{x'}}\right)$ at the trailing-edge, namely, 10^{-6} and 2×10^{-4}. The former value corresponds closely to the condition where the surface streamlines are parallel to the trailing edge, whilst the latter value is one suggested from experience in two-dimensions as the upper limit for imminent separation.

For conditions of full chord turbulent flow, Fig.11a shows that, at any given R_c, the band of possible yaw values over which separation might occur is about 5 degrees wide. When the attachment line flow is laminar the influence of the transition position is shown, in Fig.11b, to be very significant, as might be expected from two-dimensional behaviour.

The Reynolds number for separation does not rise monotonically with angle of yaw, but exhibits a minimum at roughly $\Lambda = 20^\circ$ (see Fig.11a).

This departure from a monotonic behaviour was unexpected and could be due to a number of causes. Fig.12 shows distributions of $C_{f_{x'}}$ on the upper surface as the separation boundary for $x'_{t_r}/c' = 0.0155$ is crossed along the line $R_{c'} = 10^7$ (see also Fig.11b). Away from the trailing edge the level of skin-friction falls monotonically with rising Λ, but beyond $x'/c' = 0.97$, the curves intersect giving values of $c_{f_{x'}}$ at the trailing edge that have a maximum at about $\Lambda = 20^\circ$. This corresponds to the minimum in the value of Reynolds number for separation, mentioned above.

This means that the transition assumptions give rise to initially monotonic behaviour with sweep but that the cross-flow[30] assumptions or perhaps the skin-friction assumptions[31] in the turbulent boundary-layer calculation lead to the curves of $c_{f_{x'}}$ intersecting near the trailing-edge separation condition as Fig.12 reveals.

The entrainment rate is also assumed[9] to depend upon the streamwise component of velocity defect within the boundary layer instead of the resultant velocity defect, but it is difficult to see how this approximation could lead to a behaviour that was not monotonic with sweep.

No boundary-layer treatment of the present type can yield a definition of 'significant' separation as far as the designer is concerned. Thompson, Carr-Hill and Powell[1] suggest, from the results of Jacob[19], that an error in predicted rear separation position of 3% of chord corresponds to an error of about 1% in C_L, in two-dimensional incompressible flow. Further investigation is clearly required but is outside the context of the present paper.

4.4 Surface streamline direction at the trailing edge

Fig.14 shows the variation of $\beta_{t.e.}$ with angle of yaw and Reynolds number for the upper surface of the present wing. As the cross-flow increases monotonically from the end of the rooftop to the trailing edge, this figure shows the range of angles that could be encountered in any experiment using this yawed wing. Even well away from separation, the cross-flow angles on the upper surface are likely to be large enough to allow accurate yawmeter results to be obtained. Cooke[2] used the assumption that,

$$\beta_{t.e.} = \frac{1.64 t/c \sin \Lambda \cos \Lambda}{\left(1 - M_\infty^2 \cos^2 \Lambda\right)^{\frac{1}{2}}} \quad , \tag{23}$$

which, as shown in Fig.14, leads, at $\Lambda = 45^\circ$, to a value of only 8.8°, irrespective of Reynolds number. This is much smaller than the present results. However, Cooke's value was obtained only for non-lifting symmetrical sections, and, to be fair to his pioneer work, $\beta_{t.e.}$ should be calculated from equation (23), using a value of t/c for one of his chosen family of thickness forms which would give a similar distribution of super velocity to that on the upper surface of the present aerofoil. In this case, the pressures are similar to those of a 26% thick RAE 101 thickness form, thus leading to a revised value of 16.2° for $\beta_{t.e.}$ at $\Lambda = 45^\circ$ (see Fig.14).

This value is still very much smaller than those predicted by the present method which is based upon an improved representation of the turbulent layer, and would suggest that if any separation predictions were to be based upon Cooke's expression, then they would be unreliable.

Finally, in passing, it should be noticed that the angle $\beta_{t.e.}$ at separation is not equal to $90^{\circ} - \Lambda$ as the local freestream velocity vector at the trailing edge does not in general lie in the direction of the line of flight. The difference amounts only to a few degrees and so may not be readily apparent from Fig.5, however.

4.5 The use of wind tunnel measurements as a test of the present work

Two kinds of test can be made:

(a) overall comparisons, with profile drag measurements for example, or

(b) detailed comparison with measured boundary layer and wake developments.

Furthermore, two experimental situations can be envisaged:

(c) truly infinite yawed wing conditions, or

(d) fully three-dimensional situations with gradients of mean flow not restricted in any simple quasi-two-dimensional sense.

In view of the acknowledged difficulties of achieving a closed momentum balance[21] even in nominally two-dimensional conditions it is unlikely to be worth any effort to set up experiments of type (a) + (c), whilst overall measurements of drag behind a lifting wing of type (a) + (d) are very difficult to separate into vortex and profile drag contributions.

Examination of the existing swept wing data in either of these categories confirms these difficulties. For example Dannenberg[23] measured wake traverse drags behind a high aspect ratio 45° swept wing spanning a wind tunnel, but, even in these tests, a significant spanwise pressure gradient is found except at zero lift and, in common with most early swept wing measurements, the transition front is not recorded.

Finally, in the past[26], oversimplified comparisons have been made between two-dimensional and yawed wing pressure distributions in the presence of strong viscous effects, even including separations! The rough correspondence of the $C_p \sec^2 \Lambda$ distributions is certainly not an indication that profile drag is

related to two-dimensional values as for the pressure drag alone. The pressure distributions are not coincident even without separation so that there is little reason for assuming a $\cos^3 \Lambda$ law for C_{DP}. The results quoted in Ref.26 do not prove that the rear separation position (x'/c') will be independent of Λ at a given R_c (say), because neither transition nor (possibly large) three-dimensional wall interference effects are accounted for.

Direct testing of the physics of boundary layer and wake calculation methods against detailed measurements of type (b) + (d) is the only satisfactory answer and of course need not be restricted to swept wings.

Thompson and Macdonald[4] show that the simple entrainment method employed here agrees reasonably well with measurements, nominally of type (b) + (c), described in Refs.9 and 20. However, recently, Myring[27] has suggested that the use of a better cross-flow velocity profile is necessary for adequate accuracy at higher boundary-layer Reynolds numbers, on the basis of his comparisons with data of type (b) + (d) from the experiments of East and Hoxey[28].

Earlier data for boundary layers on swept wings were not obtained in conditions close to those on an infinite yawed wing and would require lengthy analysis even where[24,25] enough profiles may have been measured. Drag could not be checked, and in the absence of information about the boundary layers on the lower surfaces, the overall displacement effect cannot be found either.

No measurements are available either for three-dimensional wakes, or for boundary layers in the region of favourable pressure gradient downstream of the attachment line on a swept leading edge. This important omission is discussed in Ref.5.

Ref.1 proposes the use of a wing with a thick symmetrical section and Warren 12 planform, at zero lift in a low-speed wind tunnel, to produce pressure gradients representative of the conditions on the upper surface of a lifting swept wing at its design point. This would be a suitable (if still rather a difficult) experiment to explore the boundary layer and wake without introducing trailing vortex or compressibility effects, thereby permitting a desirable elimination of variables.

5 CONCLUSIONS

The parametric calculations suggest, for this rooftop condition at least, that:

(i) Simple project design methods, based upon sweep factor arguments, may overestimate slightly the reduction of profile drag with sweep.

(ii) At a given streamwise chord Reynolds number, the loss of effective incidence and camber due to viscosity remains close to the value in two-dimensions until $\Lambda = 20^{\circ}$ and then increases progressively until rear separation occurs, where the additional loss of lift is about 6% of $C_L \sec^2 \Lambda$. Scale effect is amplified by yaw.

(iii) The Reynolds number for incipient trailing-edge separation rises rapidly with increasing Λ provided the attachment line flow is fully turbulent. For small angles of yaw ($\Lambda \leqslant 20^{\circ}$), when the flow is laminar at the leading edge, a slight fall in R_c is predicted for any given value of transition position. This may be a peculiarity of the turbulent boundary-layer method used here, especially in the use of the family of Mager cross-flow profiles or the Nash skin friction law.

(iv) Transition remains an important factor at typical model Reynolds numbers unless the effective leading-edge radius is much larger than for NPL 3111.

The sensitivity of the present results, therefore, to assumptions for behaviour of shape-factor or cross-flow angle at transition needs to be examined.

(v) Cross-flow angles on the upper surface are adequate for boundary-layer experiments and considerably larger, at the trailing edge, than the predictions of Cooke's simple expression (equation (23)).

A simple application of the present results for profile drag, to an idealised variable sweep wing, suggests that:

(vi) For any given flight Reynolds number ($R_{c'}$), the part of the range parameter $\frac{M_\infty L}{D_P}$, depending solely on profile drag, varies little with Λ except just before rear separation.

Finally, some overall considerations:

(vii) Although the present turbulent boundary-layer assumptions are crude, no alternative method is as yet available for design use. It would be desirable to compare the present results with a limited number of predictions from (say) the turbulence energy method.

(viii) Boundary layer and wake measurements for swept wings are still needed to provide a test of design methods.

(ix) The present conclusions (i) to (v) need verification, by direct calculation, before applying them to different forms of pressure distribution such as those with large rear loading or with leading-edge velocity peaks.

(x) The change of displacement effect with sweep angle will affect the pressure distribution and should be examined to ascertain the effect on the present conclusions, at constant $C_L \sec^2 \Lambda$ for example.

Appendix A

A PROJECT STUDY OF THE DRAG BEHAVIOUR OF AN IDEALISED VARIABLE SWEEP WING

Consider the wing shown in Fig.1b. The normal chord c', and slant length ℓ' are constant. At a given altitude ρ_∞, ν_∞, a_∞, p_∞, γ are constant, and the profile drag is given by

$$D_p = C_{DP} q_\infty c' \ell' \quad . \tag{A-1}$$

Now, $M_\infty \cos \Lambda$, $U_\infty \cos \Lambda$, are assumed to be constant and the weight and hence total lift is fixed, so that $M_\infty^2 C_L$ = constant also, compatible with the yawed wing condition. Hence,

$$q_\infty \propto \frac{1}{\cos^2 \Lambda} \quad ,$$

therefore

$$D_p \propto \frac{C_{DP}}{\cos^2 \Lambda} \quad . \tag{A-2}$$

The Reynolds number $R_{c'} = \dfrac{U_\infty \cos \Lambda c'}{\nu_\infty}$ is also constant for a given flight condition. Hence the behaviour of the wing can be summarized compactly, by contours of $R_{c'}$ on the $C_{DP}/\cos^2 \Lambda$ *versus* Λ plane. Fig.15 demonstrates this for the RAE (NPL) 3111 section at design point. A steady increase of drag with sweep is predicted assuming leading-edge transition at the lower Reynolds numbers.

Fig.16 shows the corresponding variation of that part of the range parameter which depends upon profile drag. That is,

$$\frac{D_p}{M_\infty L} = \frac{D_p \cos \Lambda}{L M_\infty \cos \Lambda} \propto D_p \cos \Lambda \propto C_{DP}/\cos \Lambda \quad . \tag{A-3}$$

A very flat minimum is found over a range of angles of yaw for all flight Reynolds numbers except very close to separation.

The complete range parameter including an approximate allowance for vortex drag may be considered as follows,

$$C_D = C_{DP} + \frac{k}{\pi A} C_L^2 \quad , \tag{A-4}$$

where, k is the vortex drag factor independent of Λ and M_∞ and only dependent on the spanwise load distribution characterised by L, ℓ and hence may be assumed fixed for any given wing. Now

$$A = \frac{\ell}{c} = \frac{\ell'}{c'} \cos^2 \Lambda = B \cos^2 \Lambda \quad , \tag{A-5}$$

where B is constant, but the aspect ratio A falls as sweep increases. Hence, for this wing of fixed area:

$$\frac{C_D}{M_\infty C_L} = \frac{1}{M_\infty C_L} \left[C_{DP} + \frac{k}{\pi B} \left[C_L^2 \right]_{2-D}^2 \cos^2 \Lambda \right]$$

$$= P \left[\frac{C_{DP}}{\cos \Lambda} + Q \cos \Lambda \right] \tag{A-6}$$

where

$$P = \frac{M_\infty \cos \Lambda}{M_\infty^2 C_L} = \frac{1}{\left[C_L \right]_{2-D} M_\infty \cos \Lambda} \tag{A-7}$$

and

$$Q = \frac{k}{\pi B} \left[C_L \right]_{2-D}^2 \tag{A-8}$$

and these are both independent of sweep.

Fig.17 shows the quantity in square brackets in (A-6) plotted against Λ for constant R_c, appropriate to a given wing and altitude etc., using the same section and taking $B = 10$, $k = 1.05$, $Q = 0.0089$.

On this basis there would appear to be a case for flying with as large a sweep angle as possible up to the limit imposed by rear separation.

This of course ignores the proper viscous/inviscid interaction behaviour which will cause loss of lift with increasing sweep and, much more fundamentally,

for the complete aircraft there will be a Mach number limit when wave drag from the fuselage becomes significant. Assuming this occurs at $M_\infty = 0.9$, this limits Λ to 42.5^o as shown on Fig.17. Distortions to the chordwise pressure distribution as well as the loading spanwise will of course occur in practice on a wing of given shape, so it is better perhaps to consider the results applied to a family of wings whose loadings retain their shape

$$\frac{c_{\ell\ell}}{c_{\ell\ell\bar{y}=0}} = f\left(\frac{\bar{y}}{\ell}\text{ , only}\right) \tag{A-9}$$

irrespective of sweep, and whose chordwise pressure distributions are held constant also.

Appendix B

THE CONDITIONS FOR CORRESPONDING INVISCID FLOW PAST A SWEPT WING AND AN UNSWEPT WING OF SIMILAR SECTION

Although the relationship between the pressure coefficients on an infinite swept wing $\left(C_{p_3}\right)$ and on the unswept wing $\left(C_{p_2}\right)$ of similar* section normal to the leading edge and equal Mach number normal to the leading edge is 'well known' (see, for example, Ref.15), *viz.*,

$$C_{p_3} = C_{p_2} \cos^2 \Lambda \quad , \tag{B-1}$$

the authors have not been able to trace its derivation. Hence, for completeness, we derive it here for all free stream conditions.

Consider two inviscid flows: the flow past an infinite unswept wing of section S at free stream Mach number $M_\infty \cos \Lambda$ and the flow past an infinite swept wing of sweep angle Λ, whose section normal to the leading edge is similar to S, at free stream Mach number M_∞. We define cartesian coordinate systems (x_2,y_2,z_2) and (x_3,y_3,z_3), where x is normal to the leading edge and y is parallel to the leading edge, and suffices 2 and 3 refer to the flows past the unswept and the swept wing respectively. Then in these systems we define velocities (u_2,v_2,w_2) and (u_3,v_3,w_3), speeds of sound a_2 and a_3, and chords normal to the leading edge c_2 and c_3.

The equations of motion for the two flows are:-

$$\left(a_2^2 - u_2^2\right) \frac{\partial u_2}{\partial x_2} + \left(a_2^2 - w_2^2\right) \frac{\partial w_2}{\partial z_2} - 2u_2 w_2 \frac{\partial u_2}{\partial z_2} = 0 \quad , \tag{B-2}$$

and

$$\left(a_3^2 - u_3^2\right) \frac{\partial u_3}{\partial x_3} + \left(a_3^2 - w_3^2\right) \frac{\partial w_3}{\partial z_3} - 2u_3 w_3 \frac{\partial u_3}{\partial z_3} = 0 \quad . \tag{B-3}$$

The distances and velocities are non-dimensionalised with respect to c_2 and V_{∞_2} in (B-2) and c_3 and $V_{\infty_3} \cos \Lambda$ in (B-3) to give:-

---

* to mean geometrically similar throughout

$$\left(\frac{a_2^2}{V_{\infty_2}^2} - u_2'^2\right)\frac{\partial u_2'}{\partial x_2'} + \left(\frac{a_2^2}{V_{\infty_2}^2} - w_2'^2\right)\frac{\partial w_2'}{\partial z_2'} - 2u_2'w_2'\frac{\partial u_2'}{\partial z_2'} = 0 \quad , \qquad \text{(B-4)}$$

and

$$\left(\frac{a_3^2}{V_{\infty_3}^2\cos^2\Lambda} - u_3'^2\right)\frac{\partial u_3'}{\partial x_3'} + \left(\frac{a_3^2}{V_{\infty_3}^2\cos^2\Lambda} - w_3'^2\right)\frac{\partial w_3'}{\partial z_3'} - 2u_3'w_3'\frac{\partial u_3'}{\partial z_3'} = 0 \quad , \qquad \text{(B-5)}$$

where non-dimensionalised quantities are dashed and the velocities at infinity in the two flows are V_{∞_2} and V_{∞_3}.

Using Bernoulli's equation for the speed of sound,

$$a^2 = a_\infty^2 + \tfrac{1}{2}(\gamma - 1)\left[V_\infty^2 - (u^2 + v^2 + w^2)\right] \quad , \qquad \text{(B-6)}$$

the following can be deduced:-

$$\frac{a_2^2}{V_{\infty_2}^2} = \frac{a_{\infty_2}^2 + \tfrac{1}{2}(\gamma - 1)\left[V_{\infty_2}^2 - \left(u_2^2 + w_2^2\right)\right]}{V_{\infty_2}^2}$$

$$= \frac{1}{M_\infty^2\cos^2\Lambda} + \tfrac{1}{2}(\gamma - 1)\left[1 - u_2'^2 - w_2'^2\right] \quad , \qquad \text{(B-7)}$$

and

$$\frac{a_3^2}{V_{\infty_3}^2\cos^2\Lambda} = \frac{a_{\infty_3}^2 + \tfrac{1}{2}(\gamma - 1)\left[V_{\infty_3}^2 - \left(u_3^2 + v_3^2 + w_3^2\right)\right]}{V_{\infty_3}^2\cos^2\Lambda}$$

$$= \frac{1}{M_\infty^2\cos^2\Lambda} + \tfrac{1}{2}(\gamma - 1)\left[1 - u_3'^2 - w_3'^2\right] \quad , \qquad \text{(B-8)}$$

since $v_3 = V_{\infty_3}\sin\Lambda$.

The boundary conditions are

$$\left.\begin{aligned} w'_s &= \frac{dS(x_s)}{dx_s}\, u'_s \quad \text{on the surface ,} \\ \text{and} \qquad & \\ u'_s &= 1 \quad \text{and} \quad w'_s = 0 \quad \text{at infinity ,} \end{aligned}\right\} \tag{B-9}$$

which are true for s equal to 2 or 3.

Therefore equations (B-4) and (B-5) are identical, and have identical boundary conditions, and so

$$u'_2 \equiv u'_3 \text{ , and } w'_2 \equiv w'_3 \text{ .} \tag{B-10}$$

Hence, from the definition of pressure coefficient,

$$C_{p_3} = \frac{2}{\gamma M_\infty^2}\left[\left(1 + \tfrac{1}{2}(\gamma - 1)M_\infty^2 \left\{1 - \frac{u_3^2 + v_3^2 + w_3^2}{V_{\infty_3}^2}\right\}\right)^{\gamma/\gamma-1} - 1\right]$$

$$= \frac{2}{\gamma M_\infty^2}\left[\left(1 + \tfrac{1}{2}(\gamma - 1)M_\infty^2 \cos^2\Lambda \left\{1 - \frac{u_3^2 + w_3^2}{V_{\infty_3}^2 \cos^2\Lambda}\right\}\right)^{\gamma/\gamma-1} - 1\right]$$

$$= \frac{2}{\gamma M_\infty^2}\left[\left(1 + \tfrac{1}{2}(\gamma - 1)M_\infty^2 \cos^2\Lambda \left\{1 - \frac{u_2^2 + w_2^2}{V_{\infty_2}^2}\right\}\right)^{\gamma/\gamma-1} - 1\right]$$

$$= C_{p_2} \cos^2\Lambda \text{ .} \tag{B-11}$$

From (B-10) and (B-11), it can be concluded that, under the conditions defined in the first paragraph, the chordwise component of velocity non-dimensionalised by the chordwise component of free stream velocity, and $C_p \sec^2\Lambda$, are both independent of sweep; these results apply to both free flight and tunnel conditions.

Appendix C

THE DERIVATION OF THE 'SWEEP FACTOR' RELATIONSHIP

The profile drag coefficient of yawed wing in a flow of free stream Mach number M_∞ and streamwise Reynolds number R_c can be split into the skin friction drag coefficient and the pressure drag coefficient $\left(C_{D_{press}}\right)$ as follows:

$$C_{DP_{3-D}} = \left[C_D - C_F\right]_{3-D} + C_{F_{3-D}} ,$$

$$= C_{D_{press}} + C_{F_{3-D}} , \qquad (C-1)$$

where the pressure drag coefficient may be written

$$C_{D_{press}} = \oint C_{p_{3-D}} d\left(\frac{z}{c'}\right) \cos \Lambda \quad . \qquad (C-2)$$

This integration takes place over the section of the wing normal to the leading edge and z is in the coordinate direction normal to the line of flight. Hence, if the flow past a similar* two-dimensional section with free stream Mach number $M_\infty \cos \Lambda$ is considered, and if it is possible to choose a Reynolds number (R) such that its displacement surface is similar to the displacement surface section normal to the leading edge of the yawed wing, then the result of Appendix B may be used to show the following:

$$\left[C_{DP} - C_F\right]_{3-D} = \oint_{\substack{\text{swept} \\ \text{wing}}} C_{p_{3-D}} d\,\frac{z}{c'} \cos \Lambda \quad ,$$

$$= \oint_{\text{2-D section}} C_{p_{2-D}} d\left(\frac{z}{c'}\right) \cos^3 \Lambda \quad ,$$

$$= \left[C_{DP} - C_F\right]_{2-D} \cos^3 \Lambda \quad . \qquad (C-3)$$

---

* This is to mean geometrically similar throughout.

Therefore, if such a Reynolds number (R) exists, the *exact* profile drag relationship is,

$$C_{DP_{3-D}}(R_c,M_\infty) = C_{F_{2-D}}(R,M_\infty \cos \Lambda)[\lambda_E - 1] \cos^3 \Lambda + C_{F_{3-D}}(R_c,M_\infty) \quad , \quad (C-4)$$

where

$$\lambda_E = \lambda_E(R,M_\infty \cos \Lambda) = \frac{C_{DP_{2-D}}(R,M_\infty \cos \Lambda)}{C_{F_{2-D}}(R,M_\infty \cos \Lambda)} \quad . \quad (C-5)$$

Now, in the main part of this paper, only one physically realistic flow is known. That is, the flow at $\Lambda = 0^o$, for $R = 15.6 \times 10^6$, described by Firmin and Cook[17]. If however, a set of (R_c,Λ) can be found such that the $\delta^*_u/c'(x'/c')$ and $\delta^*_L/c'(x'/c')$ distributions are identical, then this set of flows is physically consistent and the total displacement shapes are similar. If the set of (R_c,Λ) chosen is that for which the incidence change is constant, that is, if

$$\Delta\alpha(R = 15.6 \times 10^6, \Lambda = 0^o) \equiv \Delta\alpha(R_c,\Lambda) \sec \Lambda \quad ,$$

then by considering this line $(\Delta(\alpha \sec \Lambda) = 0.195^o)$, the intersections with contours of R_c in Fig.10 give values of Λ for which the displacement surfaces are indeed nearly similar. Hence, equation (C-4) holds almost exactly there.

A swept wing drag relationship of the type often used by Project Offices[3] can be obtained as follows:-

The profile drag of the section perpendicular to the leading edge and the skin friction drag of the section at zero Mach number and same streamwise Reynolds number are related by:-

$$C_{DP_{2-D}}(R_c,M) = \lambda_{W_{2-D}} \times C_{F_{plate}}(R_c,0) \quad . \quad (C-6)$$

If equation (C-6) is used to determine $C_{DP_{2-D}}$ from $C_{F_{2-D}}$, it is normally assumed that λ_W is a function of section shape only (say, t/c and $\partial C_L/\partial\alpha$),

and not of Mach number (below the drag rise Mach number). Alternatively, equation (C-6) may be used to calculate λ_W from knowledge of $C_{DP_{2-D}}$.

The form factor concept may be extended to swept wings by following an empirical correlation of Cookes[2] calculated results to give

$$\lambda_{W_{3-D}}(M) = \left\{\lambda_{W_{2-D}}(M \cos \Lambda) - 1\right\} \cos^3 \Lambda + 1 \quad . \qquad (C-7)$$

Therefore, the following swept wing drag relationship may be written:-

$$C_{DP_{3-D}}(R_c,M) = \left[\left\{\lambda_{W_{2-D}}(M \cos \Lambda) - 1\right\} \cos^3 \Lambda + 1\right] \times C_{F_{plate}}(R_c,0) \quad . \qquad (C-8)$$

Comparison of equations (C-4) and (C-8) shows that the approximate equation has the correct general structure, and, in order to obtain some estimate of the errors involved in using equation (C-8), the two equation relationships have been compared for the particular set of operating conditions specific to this paper for which the relationship (C-4) holds almost exactly (i.e. $\Delta\alpha \sec \Lambda = 0.195^{\circ}$). It is found that even in the worst case, the error on drag coefficient is only -2%.

It is seen (Fig.6) that the errors in using equation (C-8) over the whole range of (R_c,Λ) considered (though admittedly the flows considered, apart from those mentioned above, are not quite physically realistic) are between $-2\frac{1}{2}\%$ and $+1\frac{1}{2}\%$.

NOTATION

A	aspect ratio
c'	chord length normal to leading edge
c	chord length in line of flight
c_f	local coefficient of skin friction
$c_{f_{x'}}$	component of local coefficient of skin friction in chordwise direction
c_{LL}	local lift coefficient per unit span
C^*	$\left(= \dfrac{U_\infty^2 \sin^2 \Lambda}{\nu_{a.l.} \, dU_1/ds'} = \dfrac{\sigma'}{2c'} R_{c'} \dfrac{\nu_\infty}{\nu_{a.l.}} \tan^2 \Lambda \right)$, the similarity parameter of attachment line flow
C_{DP}	profile drag coefficient
C_F	coefficient of drag due to integrated skin-friction across chord
C_L	lift coefficient
C_p	local pressure coefficient
D	total drag force
F	entrainment coefficient
F_c, F_r	functions in Spalding-Chi skin-friction law
G	$\sqrt{\dfrac{2}{c_{f_1}}} \dfrac{\int_0^\infty (U_e - u)^2 dz}{\int_0^\infty (U_e - u) dz}$
$\bar{H}$	$= \dfrac{1}{\theta_{11}} \int_0^\infty \dfrac{\rho}{\rho_e} \left(1 - \dfrac{u}{U_e}\right) dz$, compressible analogue of H
H_1	$= \dfrac{(\delta - \delta_1^*)}{\theta_{11}}$
H	$= \dfrac{\delta_1^*}{\theta_{11}}$
k	induced drag factor
ℓ	span
ℓ'	slant length of wing parallel to generators
L	total lift force
M	Mach number

NOTATION (continued)

q	$(= \frac{1}{2}\rho U^2)$ dynamic pressure
$R_{c'}$	$\left(= \frac{U_\infty \cos \Lambda c'}{\nu_\infty}\right)$ chordwise chord Reynolds number
R_c	$\left(= \frac{U_\infty c}{\nu_\infty} = R_{c'} \sec^2 \Lambda\right)$ streamwise chord Reynolds number
$R_{\theta_{11}}$	$\left(= \frac{U_e \theta_{11}}{\nu_e}\right)$ streamwise momentum thickness Reynolds number
s	distance along an external streamline started at a small distance ε from the attachment line
s'	distance around surface of wing in chordwise plane, measured from the attachment line at the leading edge
T	local static temperature
u	velocity in the U_e direction inside the boundary layer
U_e	external velocity
U_1	component of external velocity in chordwise plane
v	cross-flow velocity, normal to U_e
$\bar{x},\bar{y},\bar{z}$	rectangular Cartesian coordinates with $\bar{x}$ along line of flight, $\bar{z}$ normal to wing plane
x',y',z'	rectangular Cartesian coordinates with x' chordwise, y' spanwise, z' normal to wing plane
	For local boundary layer expressions we use rectangular coordinates with z normal to the surface and either s or s' with the appropriate third normal coordinate (y or y')
α	angle of incidence
β	angle between surface streamline and local external streamline directions
δ	value of z for which the total velocity within the boundary layer = $0.995U_e$
δ_1^*	$\left(= \int_0^\delta \left(1 - \frac{\rho u}{\rho_e U_e}\right) dz\right)$ conventional definitions
δ_2^*	$\left(= - \int_0^\delta \frac{\rho v}{\rho_e U_e} dz\right)$ conventional definitions
$\Delta( )$	change of quantity inside brackets
λ_W	$\left(= \frac{C_{DP}}{C_{F_{plate}}}\right)$ aerofoil form factor, see Appendix C
Λ	angle of yaw

NOTATION (concluded)

ρ fluid density

σ' 'effective' leading edge radius of the chordwise section (i.e. the radius of the circular cylinder that, in incompressible flow, has the same velocity gradient as at the attachment line of the aerofoil), used to find C^*.

ν fluid kinematic viscosity

ϕ angle between $\underline{U_e}$ and $\underline{s'}$

θ_{11} $\left(= \int_0^\delta \frac{\rho u}{\rho_e U_e} \left(1 - \frac{u}{U_e}\right) dz \right)$

θ_{12} $\left(= \int_0^\delta \frac{\rho v}{\rho_e U_e} \left(1 - \frac{u}{U_e}\right) dz \right)$

θ_{21} $\left(= - \int_0^\delta \frac{\rho}{\rho_e} \left(\frac{uv}{U_e^2}\right) dz = \theta_{12} + \delta_2^* \right)$

θ_{22} $\left(= - \int_0^\delta \left(\frac{v}{U_e}\right)^2 \frac{\rho}{\rho_e} dz \right)$

conventional definitions based on streamline coordinates.

Subscripts:

a.l. conditions at the attachment line

∞ conditions at infinity

t.e. trailing edge value

e local resultant free stream value

3-D value for the swept wing

2-D value for chordwise section in two-dimensional flow (i.e. unyawed)

tr value at transition point

U,L upper, lower surface values, respectively

l.e. leading edge value

t turbulent value, just after transition

ℓ laminar value, just before transition

plate value for a flat plate

Superscripts:

' in chordwise plane, e.g. θ', x'

s spanwise component, e.g. θ^s

REFERENCES

No.	Author	Title, etc.
1	B.G.J. Thompson G.A. Carr-Hill B.J. Powell	A programme of research into viscous aspects of flow on swept wings. NPL Aero Note 1100 (ARC 32402), October 1970
2	J.C. Cooke	The drag of infinite swept wings. With an Addendum ARC CP No.1040 (1964)
3	J.E. Rossiter	A suggested framework for the analysis and synthesis of the drag of wing-body combinations at subsonic speeds. Private communication
4	B.G.J. Thompson A.G.J. Macdonald	The prediction of boundary layer behaviour and profile drag for infinite yawed wings. Part I: A method of calculation. ARC CP No. 1307 (1973)
5	B.G.J. Thomspon	The prediction of boundary layer behaviour and profile drag for infinite yawed wings. Part II: Flow near a turbulent attachment line. ARC CP No. 1308 (1973)
6	B. Thwaites	Approximate calculation of the laminar boundary layer. Aero. Quart, Vol.1, pp.245-280 (1949)
7	N. Rott	Compressible laminar boundary layer on a heat-insulated body. Journ. Aero. Sci., pp.67-68, January 1953
8	G. Nath	The compressible laminar spanwise boundary layer on a yawed infinite cylinder with distributed suction. Acta. Tech. Acad. Sci. Hung., 56(1-2), pp.187-198 (1966)
9	N.A. Cumpsty M.R. Head	The calculation of three-dimensional turbulent boundary layers. Pt.1: Flow over the rear of an infinite swept wing. Aero. Quart. Vol.18, Pt.1, pp.55-84, February 1967

REFERENCES (continued)

No.	Author	Title, etc.
10	N.A. Cumpsty M.R. Head	The calculation of three-dimensional turbulent boundary layers. Pt.2: Attachment-line flow on an infinite swept wing. Aero. Quart. Vol.18, Pt.2, pp.150-164, May 1967
11	N.A. Cumpsty M.R. Head	The calculation of three-dimensional turbulent boundary layers. Pt.3: Comparison of attachment-line calculations with experiment. Aero. Quart. Vol.20, Pt.2, pp.99-113, May 1969
12	N.A. Cumpsty M.R. Head	The calculation of three-dimensional turbulent boundary layers. Pt.4: Comparison of measurement with calculations on the rear of a swept wing. Brit. Aero. Res. Council, CP No.1077. Aero. Quart. Vol.21, Pt.2, pp.121-132, May 1970
13	J.E. Green	The prediction of turbulent boundary layer development in compressible flow. J.F.M. Vol.31, Pt.4 (1968)
14	J.F. Nash J. Osborne A.G.J. Macdonald	A note on the prediction of aerofoil profile drag at subsonic speeds. NPL Aero Report 1196 (ARC 28075) (1966)
15	R.C. Lock	An equivalence law relating three- and two-dimensional pressure distributions. NPL Aero. Report 1028 (ARC 23952) July 1962
16	T.A. Cook	Private communication
17	M.C.P. Firmin T.A. Cook	Detailed exploration of the compressible viscous flow over two-dimensional aerofoils at high Reynolds numbers. Sixth Congress ICAS, Paper No.68-09, September 1968
18	A.D. Young T.B. Booth	The profile drag of yawed wings of infinite span. The Aeronaut. Quart. Vol.3, p.211 (1951)
19	K. Jacob	Theoretical calculation of pressure distribution and force coefficients for any profile in incompressible flow with separation. Min. Tech. translation T6205 of AVA Report 67A62. ARC 31936 (1966)

REFERENCES (continued)

No.	Author	Title, etc.
20	P. Bradshaw	Calculation of three-dimensional turbulent boundary layers. J.F.M. Vol.46, Pt.3, pp.417-445 (1971)
21	B.G.J. Thompson	A critical review of existing methods of calculating the turbulent boundary layer. ARC R & M 3447 (1964)
22	J.C. Cooke	Note on three-dimensional boundary-layer transition. (ARC 23672) March 1962
23	R.E. Dannenberg	Measurements of section characteristics of a 45^{o} swept wing spanning a rectangular low-speed wind tunnel as affected by the tunnel walls. NACA TN2160 (1950)
24	G.C. Brebner L.A. Wyatt	Boundary layer measurements at low speed on two wings of 45^{o} and 55^{o} sweep. ARC CP No.554 (1960)
25	R.E. Wallace	The experimental investigation of a swept-wing research model boundary layer. Univ. of Wichita, School of Engineering, Aero. Dept. Report 092, January 1953
26	R.C. Lock E.W.E. Rogers	Aerodynamic design of swept wings and bodies for transonic speeds. Proceedings 2nd I.C.A.S. Zurich, September 1960
27	D.F. Myring	An integral prediction method for three-dimensional turbulent boundary layers in incompressible flow. RAE Technical Report 70147 (ARC 32647) (1970)
28	L.F. East R.P. Hoxey	Low-speed three-dimensional turbulent boundary layer data. Pt.1 ARC R & M 3653 (1969) Pt.2 RAE Technical Report 69137 (ARC 31721) (1969)

REFERENCES (continued)

No.	Author	Title, etc.
29	-	The compressible two-dimensional turbulent boundary layer, both with and without heat transfer, on a smooth flat plate, with application to wedges, cylinders and cores. ESDU A106D, September 1968
30	A. Mager	Generalisation of boundary-layer momentum equations to three-dimensional flows, including those of rotating systems. NACA Report 1067 (1952)
31	J.F. Nash A.G.J. Macdonald	A turbulent skin-friction law for use at subsonic and transonic speeds. ARC CP. No.948 (1966)
32	J.C. Cooke M.G. Hall	Boundary layers in three dimensions. RAE Report Aero 2635 (ARC 21905) (1960)
33	P.D. Smith	A calculation method for the compressible turbulent boundary layer on an infinite yawed wing on compressible adiabatic flow. ARC CP No. 1268 (1972)
34	B.G.J. Thompson	The prediction of shape-factor development in incompressible turbulent boundary layers with or without transpiration. AGARDograph 97, pp.159-190 (1965)
35	B.G.J. Thompson	A new two-parameter family of mean velocity profiles for incompressible turbulent boundary layers on smooth walls. ARC R & M 3463 (1965)
36	J.E. Green	Application of Head's entrainment method to the prediction of turbulent boundary layers and wakes in compressible flow. RAE Technical Report 72079 (ARC 34052) (1972)
37	J.E. Green	The turbulent boundary layer in two-dimensional flows with an oblique shock wave. Ph.D. thesis Univ. of Cambridge Dept. Engineering (1966)

REFERENCES (concluded)

No.	Author	Title, etc.
38	D.B. Spalding S.W. Chi	The drag of a compressible turbulent boundary on a smooth flat plate with and without heat transfer. J.F.M. Vol.18, p.118 (1964)
39	P.D. Chappell M.D. Hodges	Note on the effect of wake treatment on profile drag predictions using the J.F. Nash boundary layer development. Roy. Aero. Soc. ESDU, Item A150 (1967)

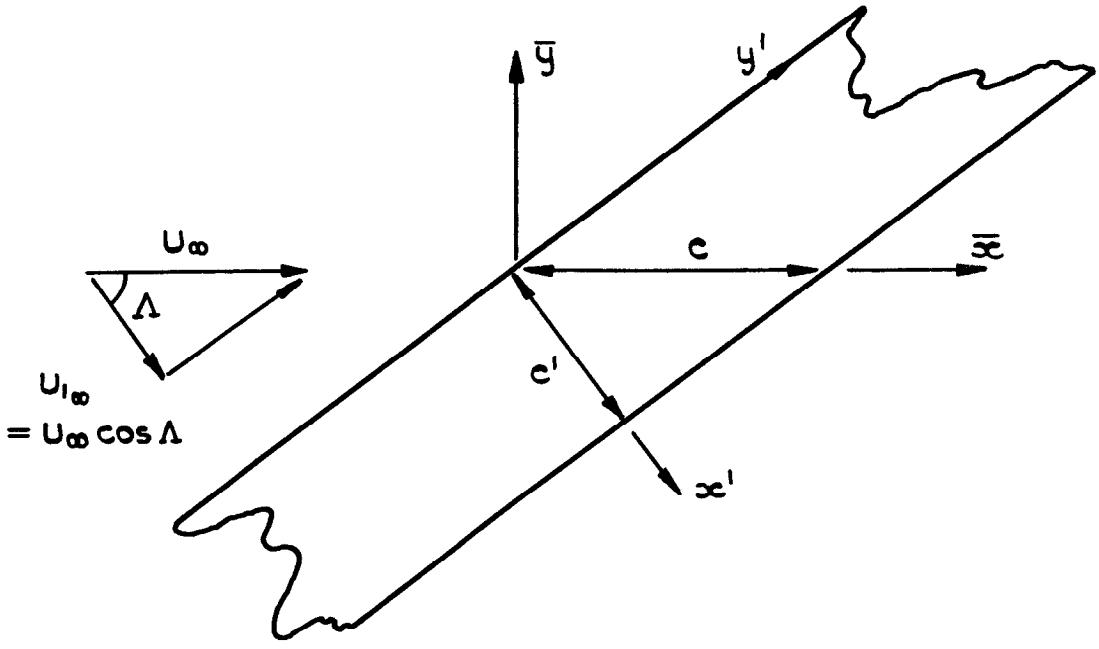

Fig.1a Definition sketch for infinite yawed wing

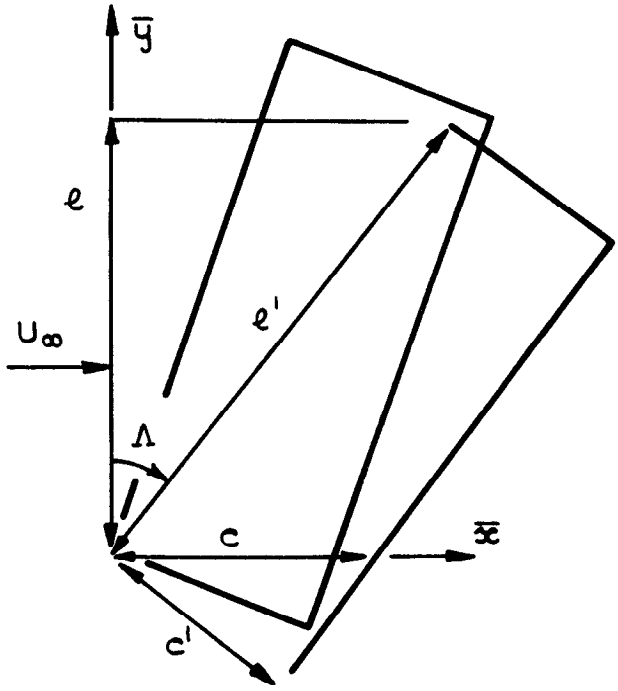

Fig.1b Definition of variable sweep wing, used in Fig.15,16,17

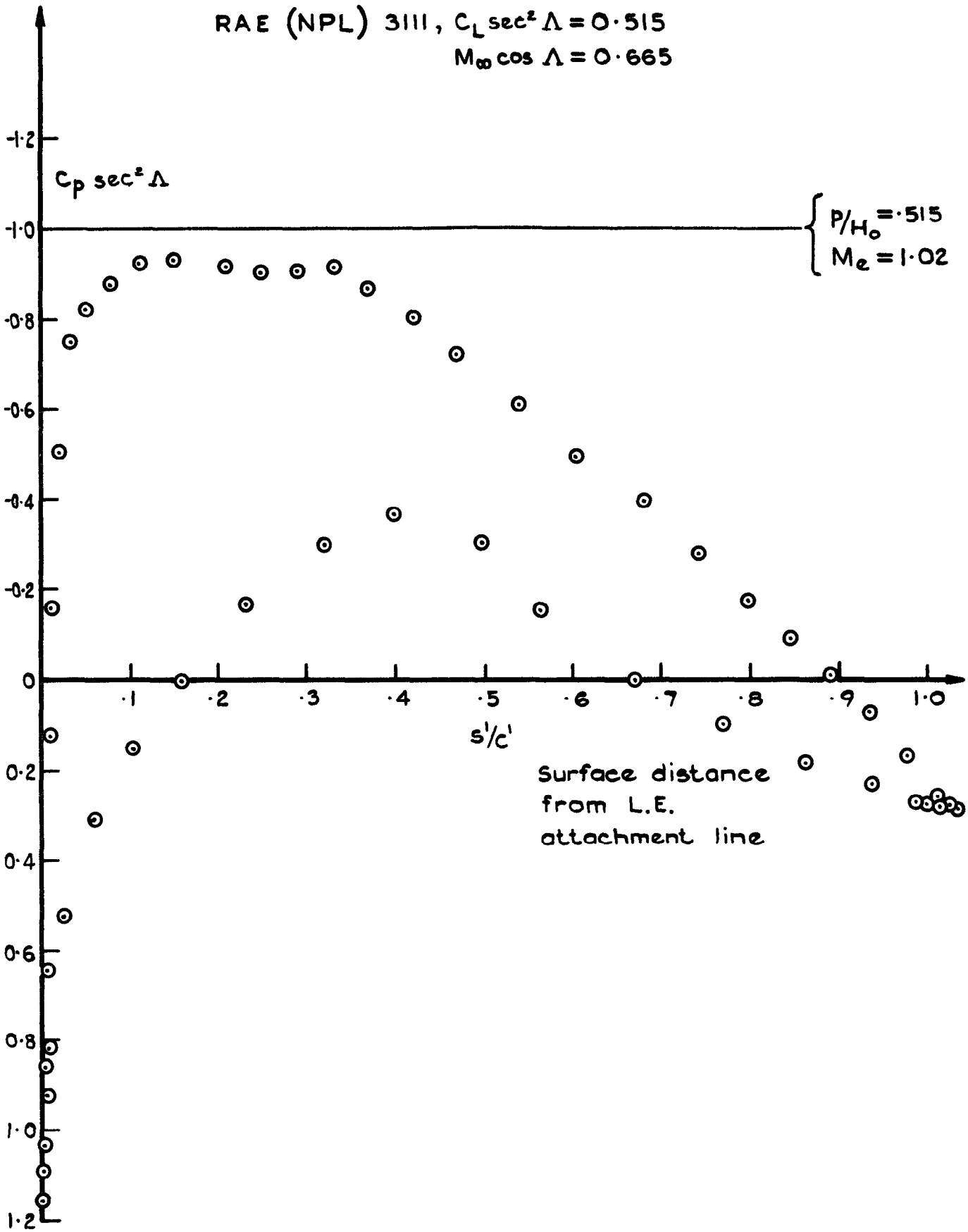

Fig. 2 Chordwise pressure distribution for the two-dimensional section used in the parametric calculations of the effects of yaw

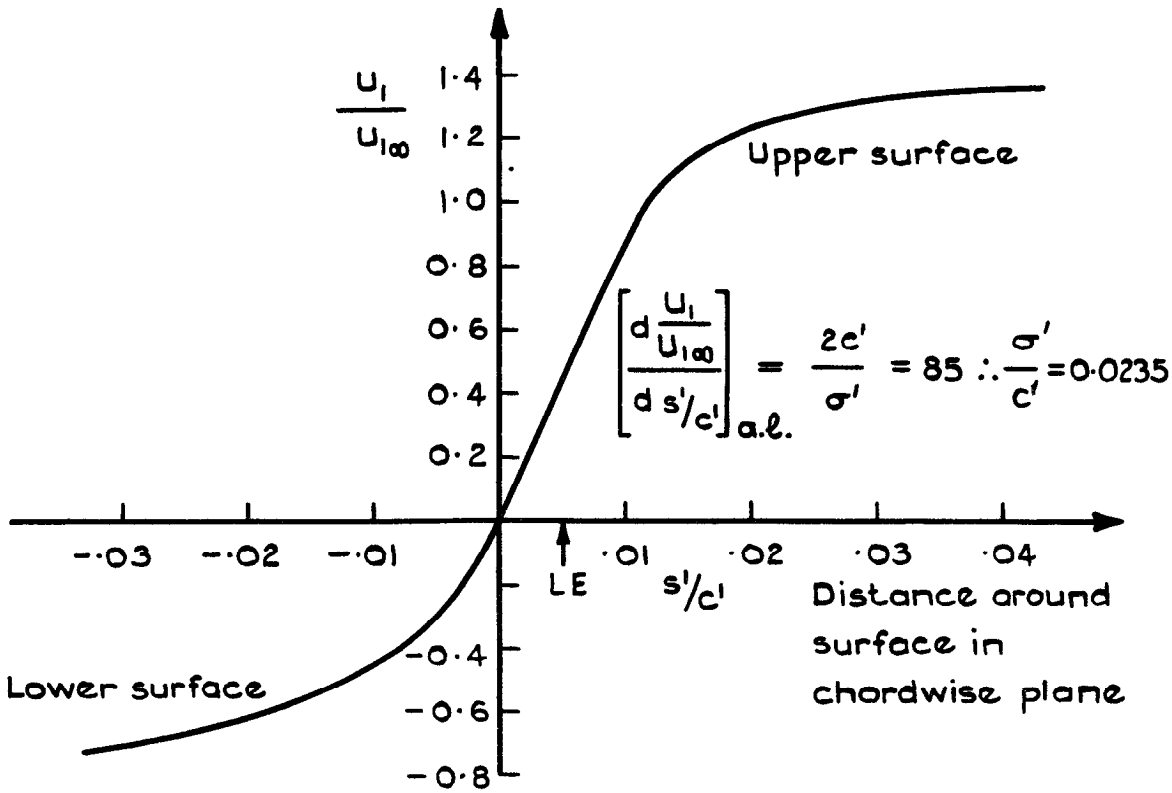

Fig. 3 Detailed distribution of chordwise velocity component around leading edge

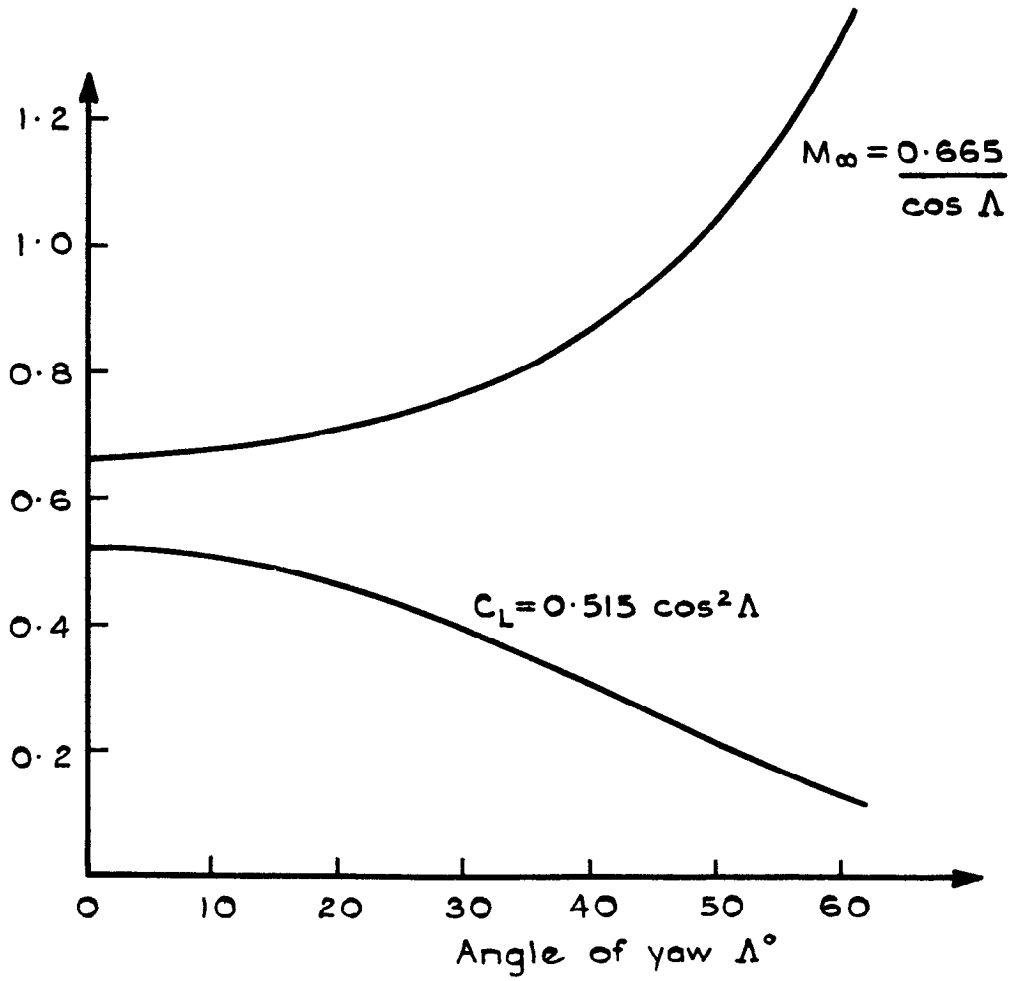

Fig. 4 Operating conditions for yawed wing at section design point of RAE (NPL) 3111

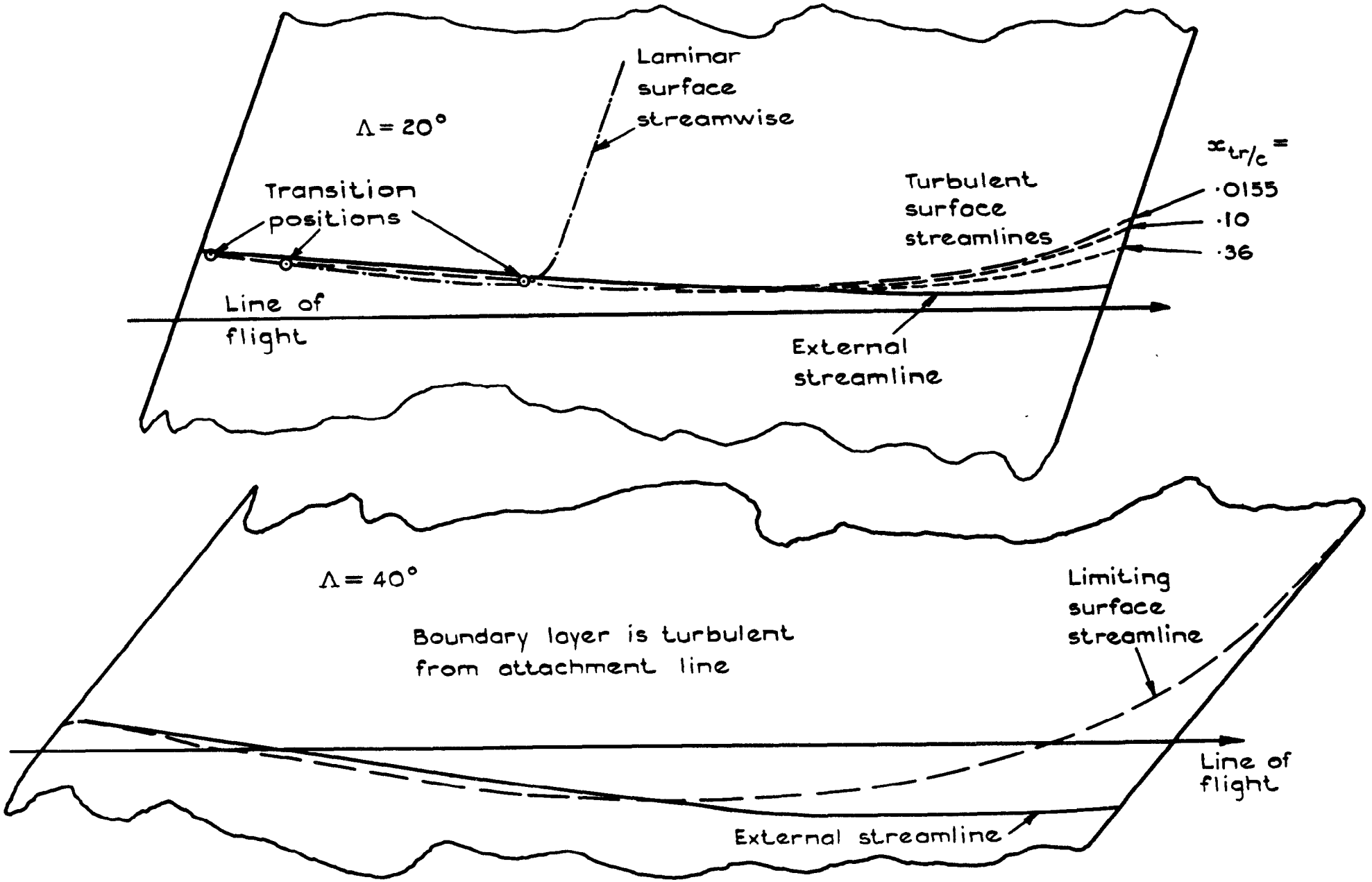

Fig.5 Typical upper surface streamlines at $R_c = 2 \times 10^7$

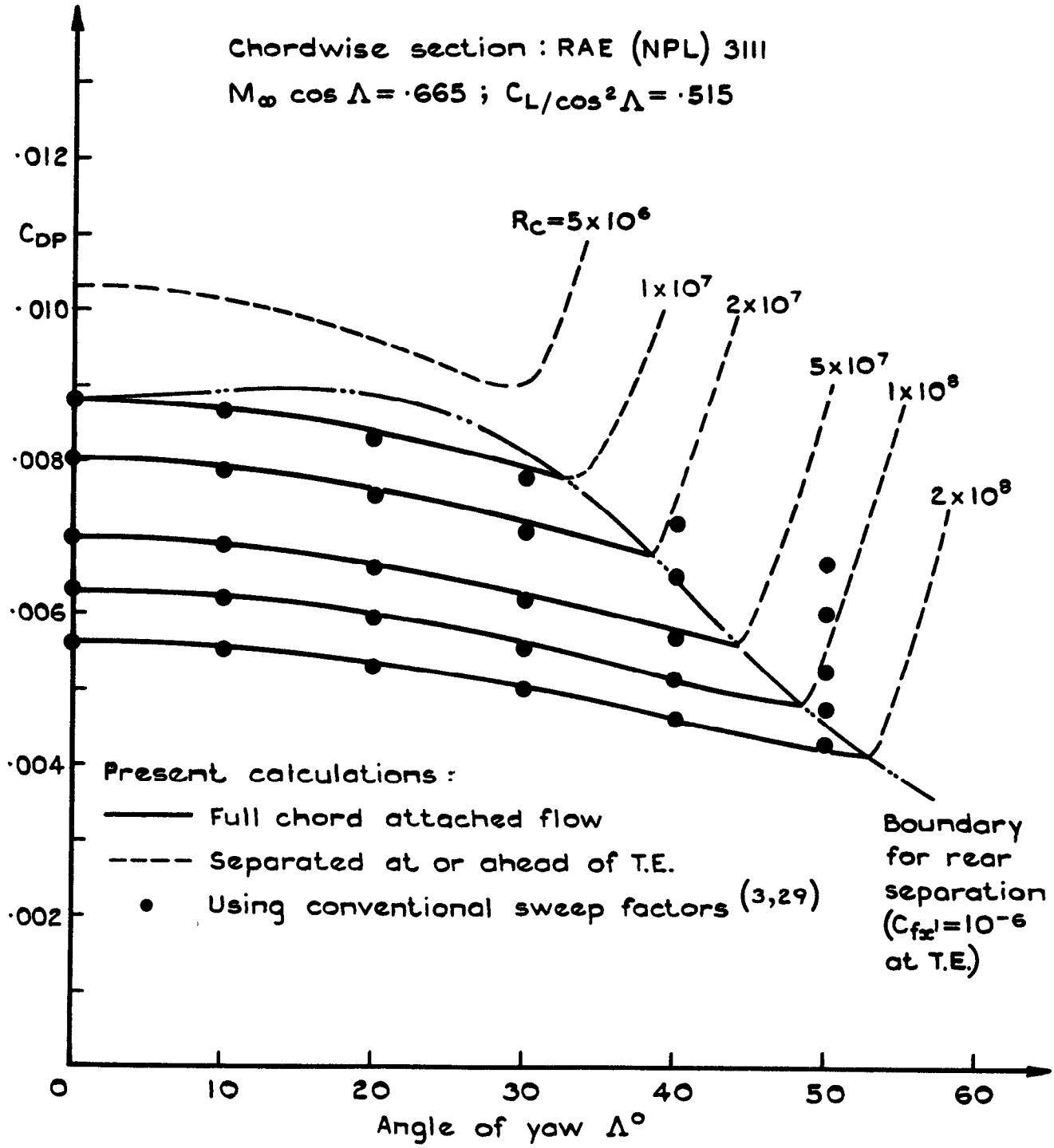

Fig. 6 Variation of profile drag with yaw and streamwise chord Reynolds number for "Leading edge" turbulent flow

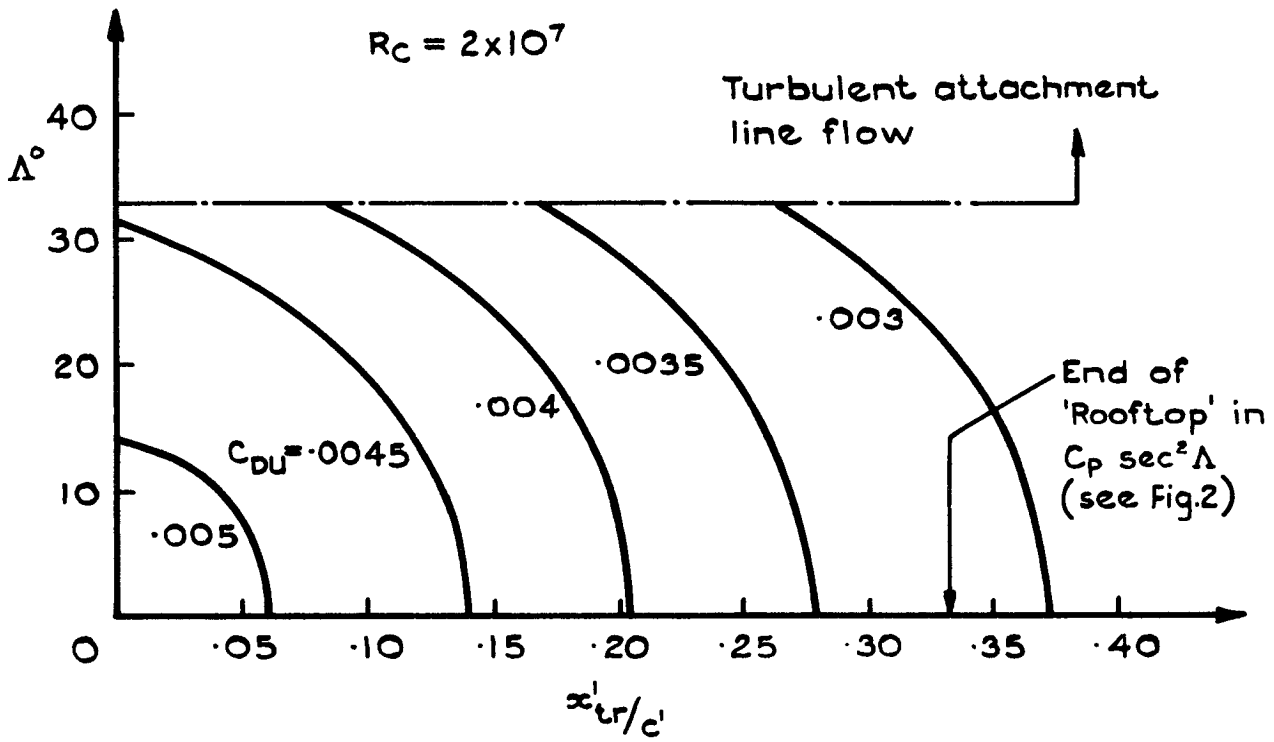

Fig.7 Exchange between angle of yaw and transition position for given values of upper surface profile drag

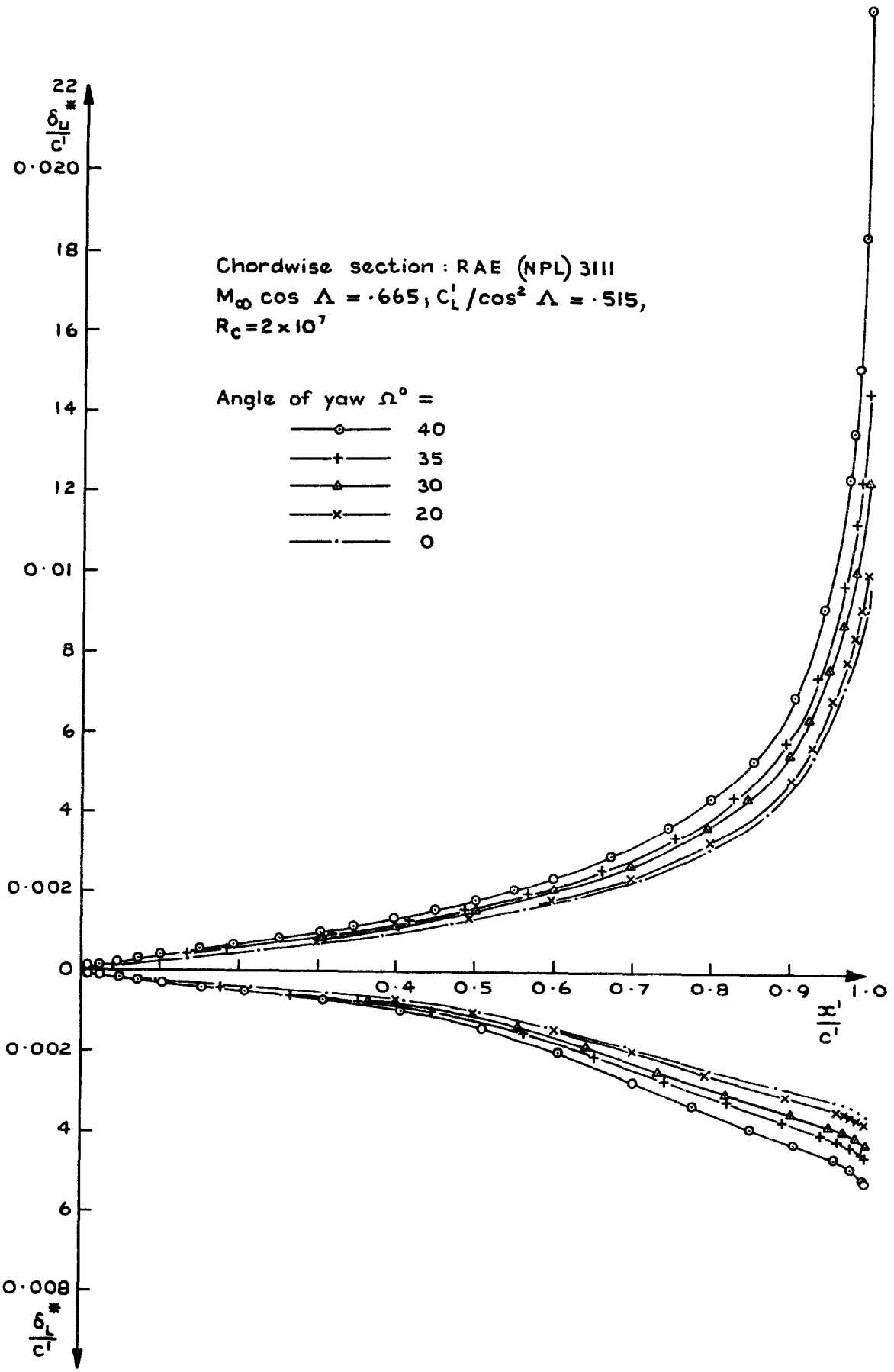

Fig.8 Variation of the distribution of displacement thickness with angle of yaw at a constant streamwise chord Reynolds number, and "Leading edge" transition

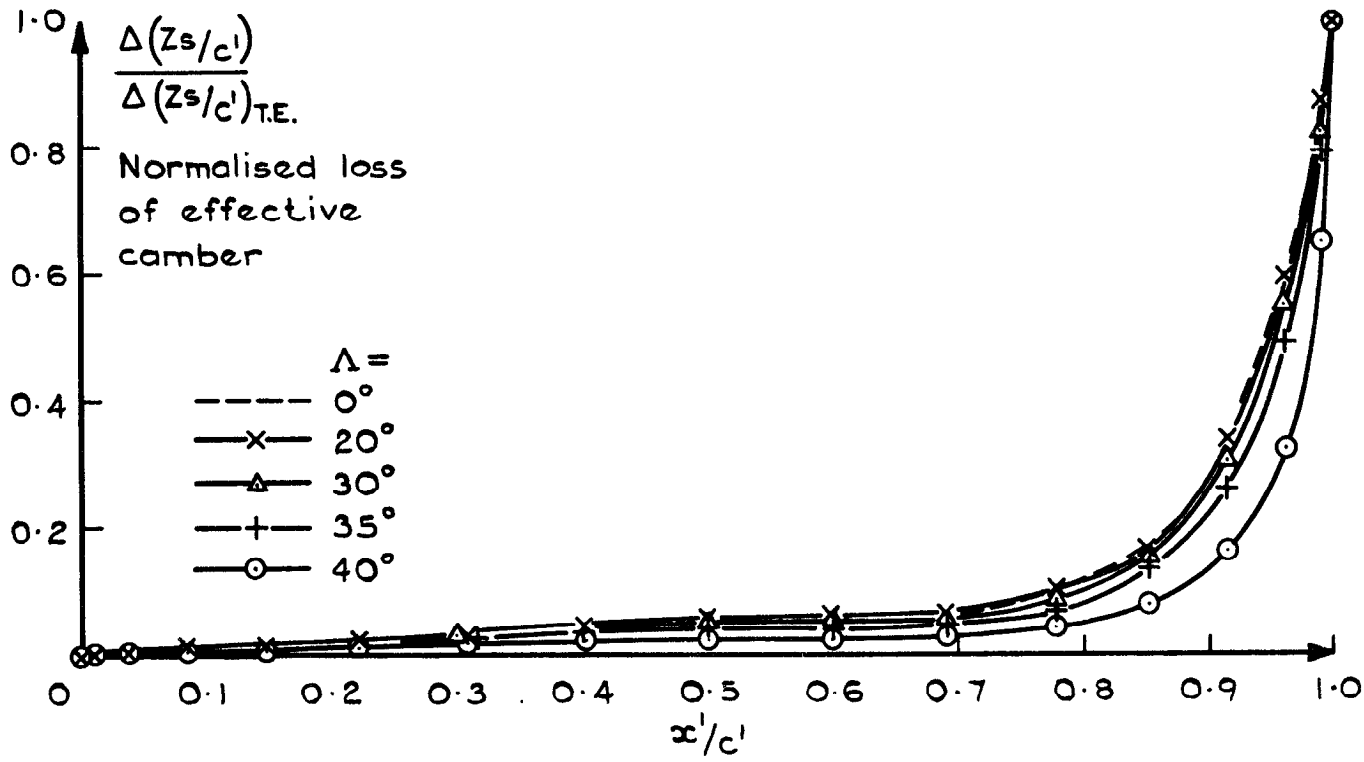

Fig. 9 Comparison of distributions of camber loss due to viscosity – (normalised on trailing edge values) – conditions of Fig. 8

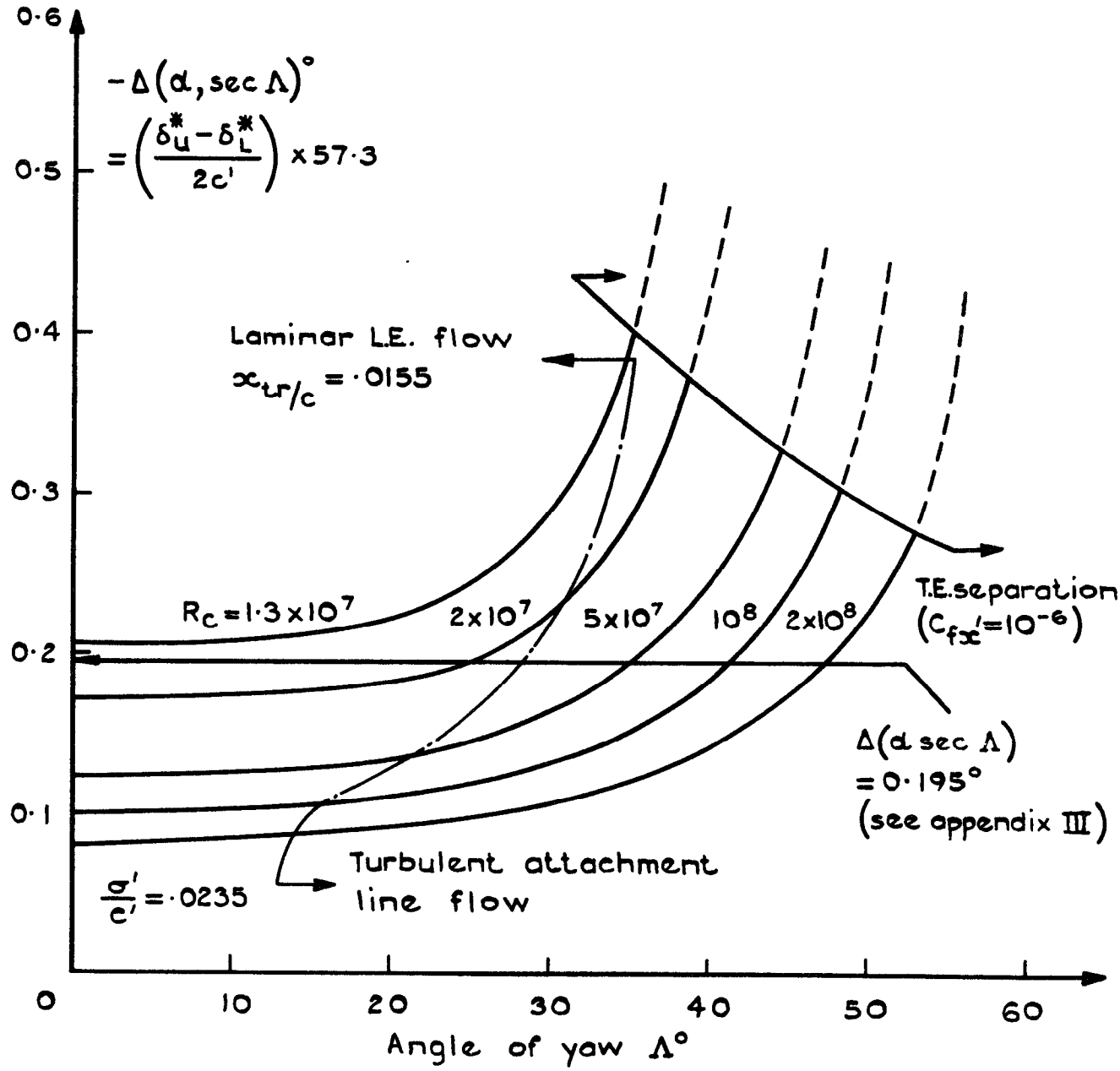

Fig. 10 Variation of viscous effect, on incidence, with yaw and Reynolds number. (Chordwise section : RAE (NPL) 3111 $(\alpha - \alpha_{C_L=0})$ see $\Lambda = 3{\cdot}6^\circ$, $M_\infty \cos\Lambda = 0{\cdot}665$, $C_L \sec^2\Lambda = 0{\cdot}515$)

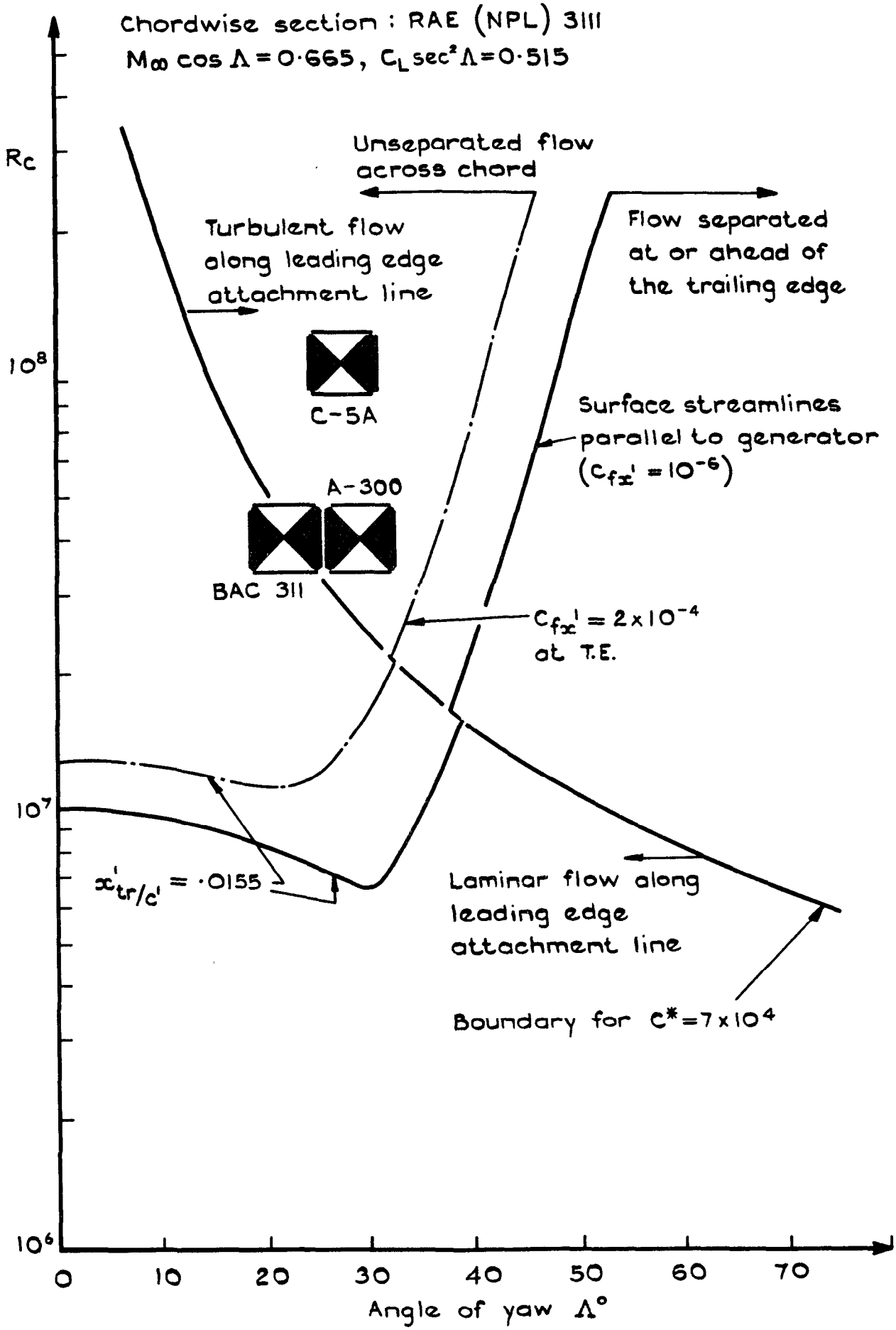

Fig. IIa Variation of incipient trailing edge separation with yaw for "Full chord" turbulent flow

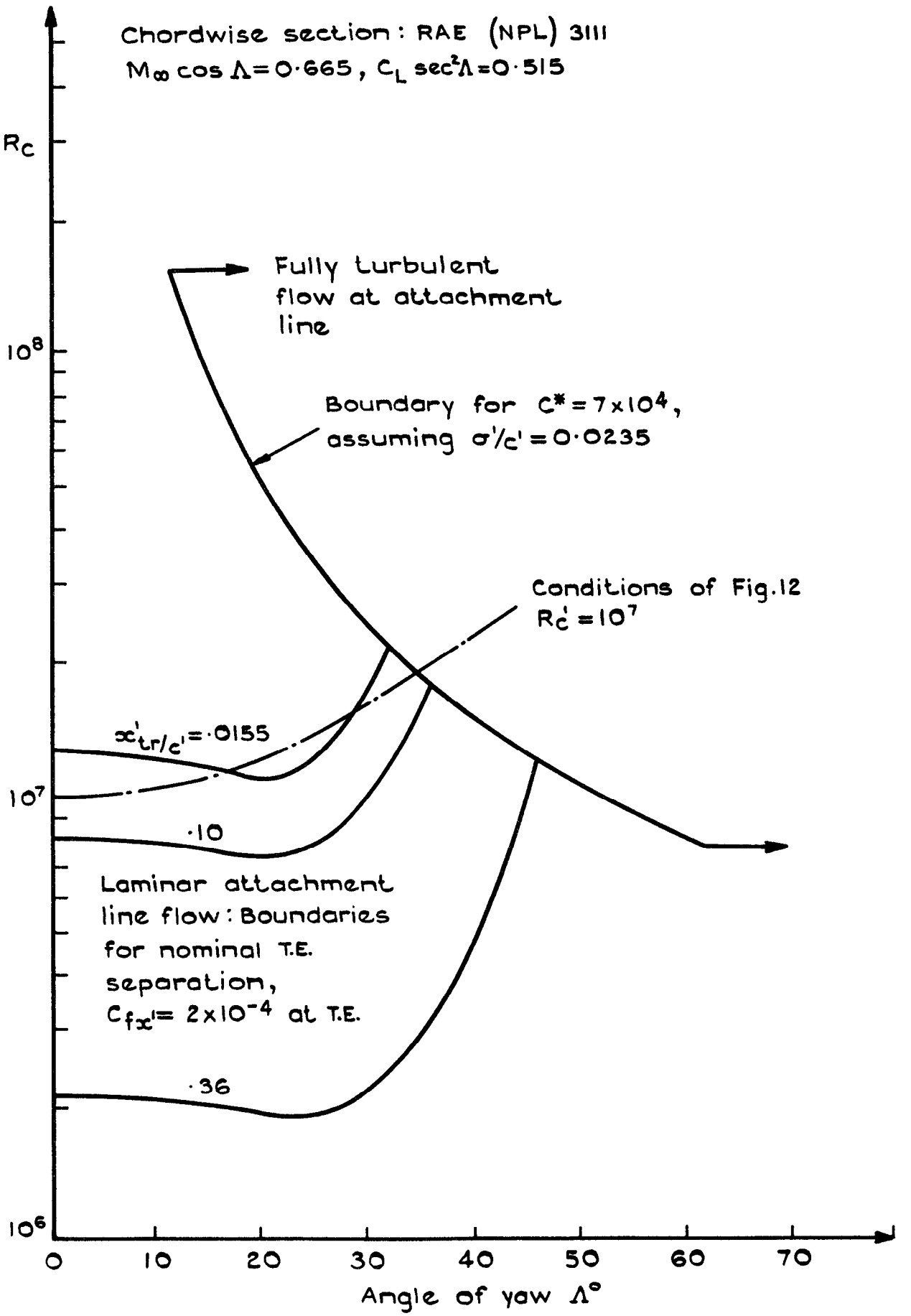

Fig. 11b Variation of incipient trailing edge separation with yaw and transition position

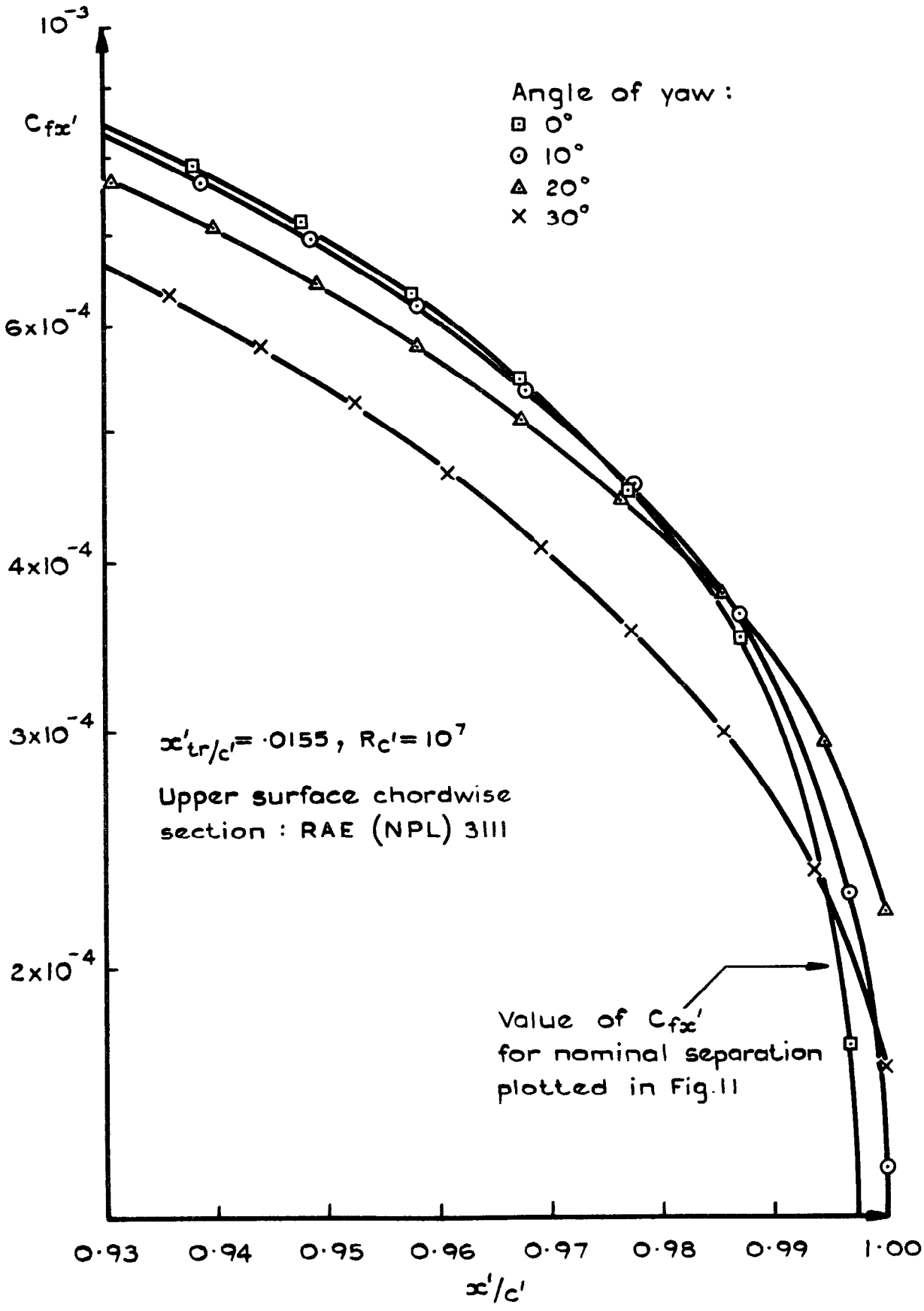

Fig.12 Variation of chordwise component of skin-friction with angle of yaw

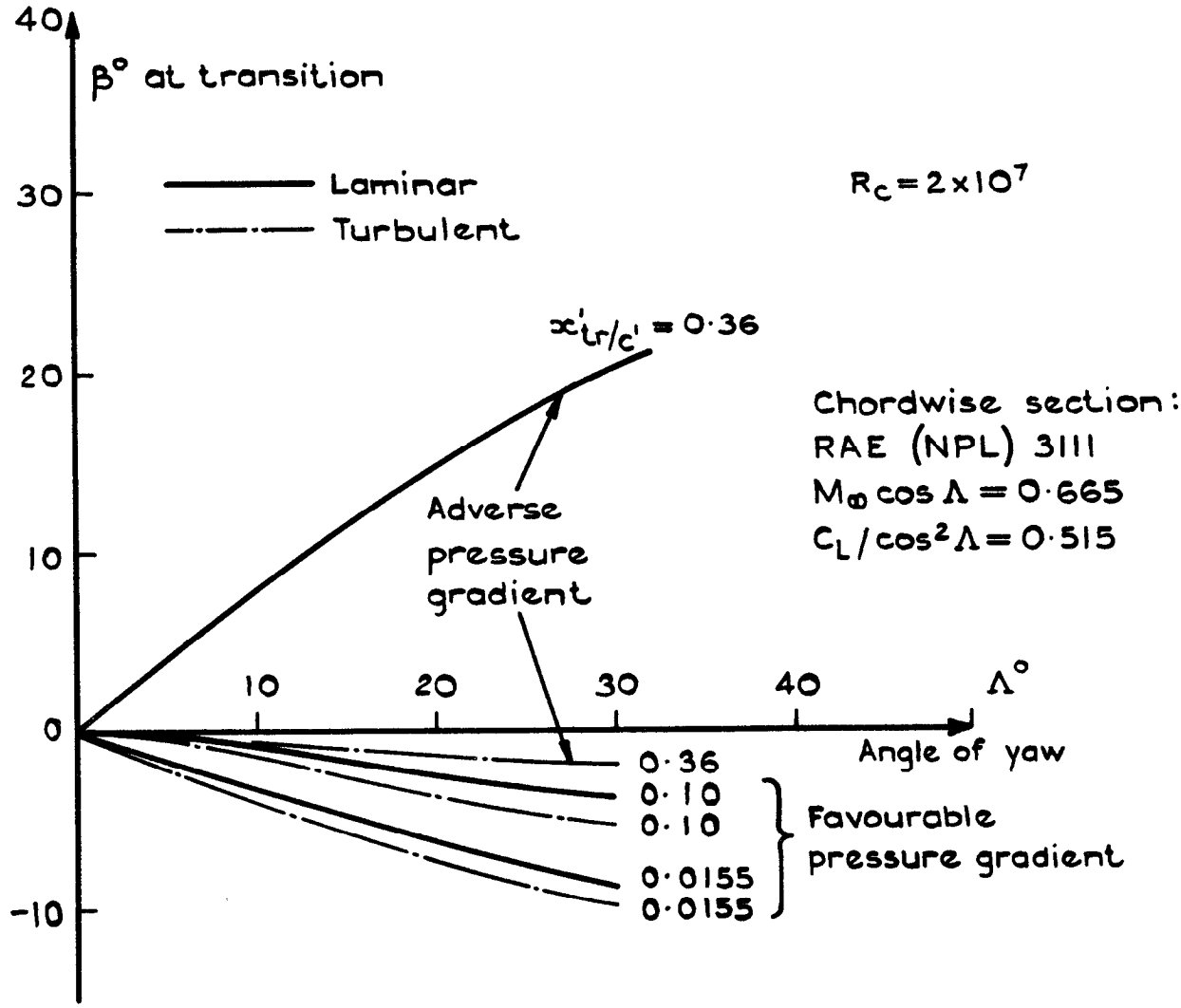

Fig.13 Behaviour of crossflow at transition according to present assumptions

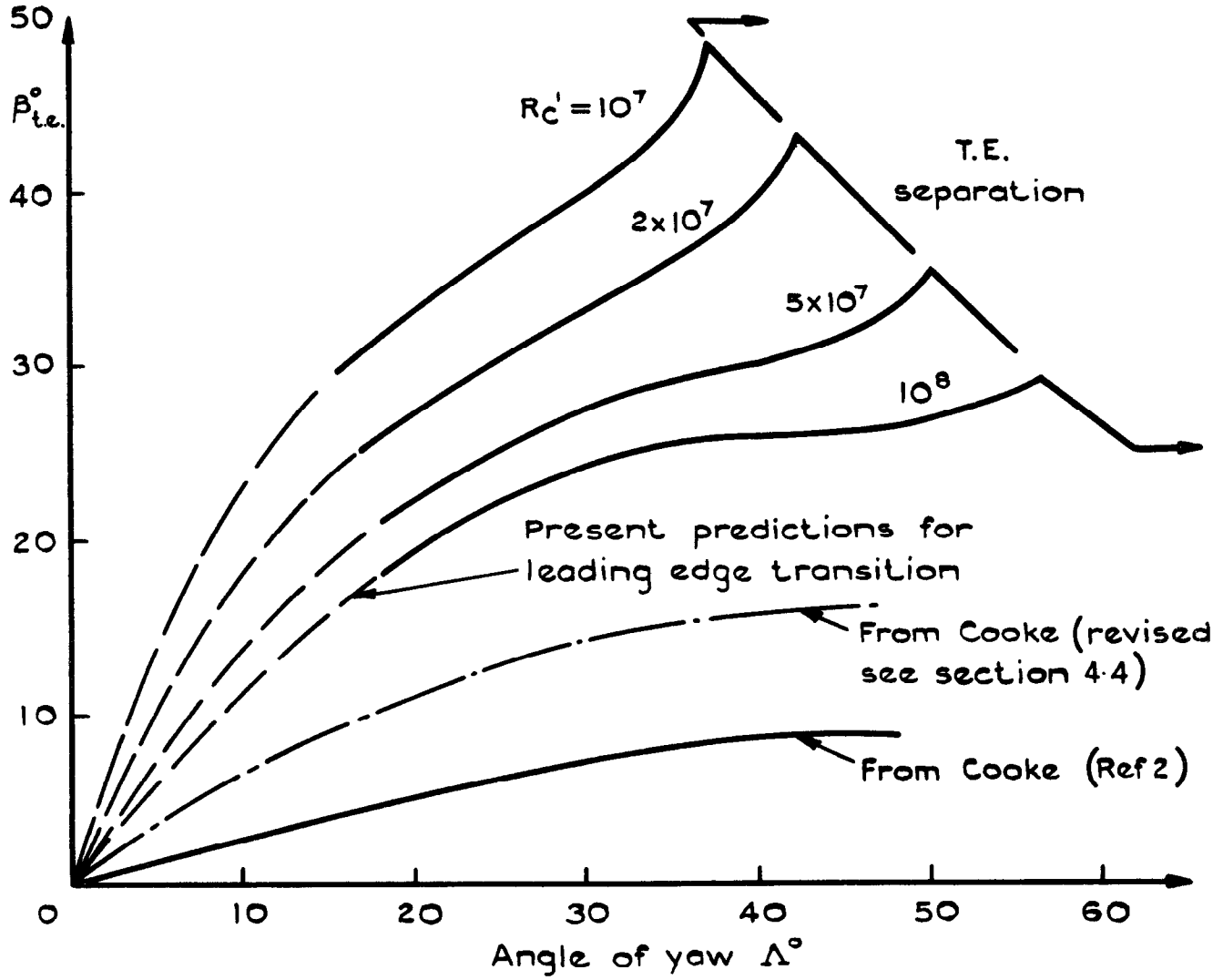

Fig.14 Effect of yaw on upper surface crossflow angle at the trailing edge, for RAE (NPL) 3111 section at design condition

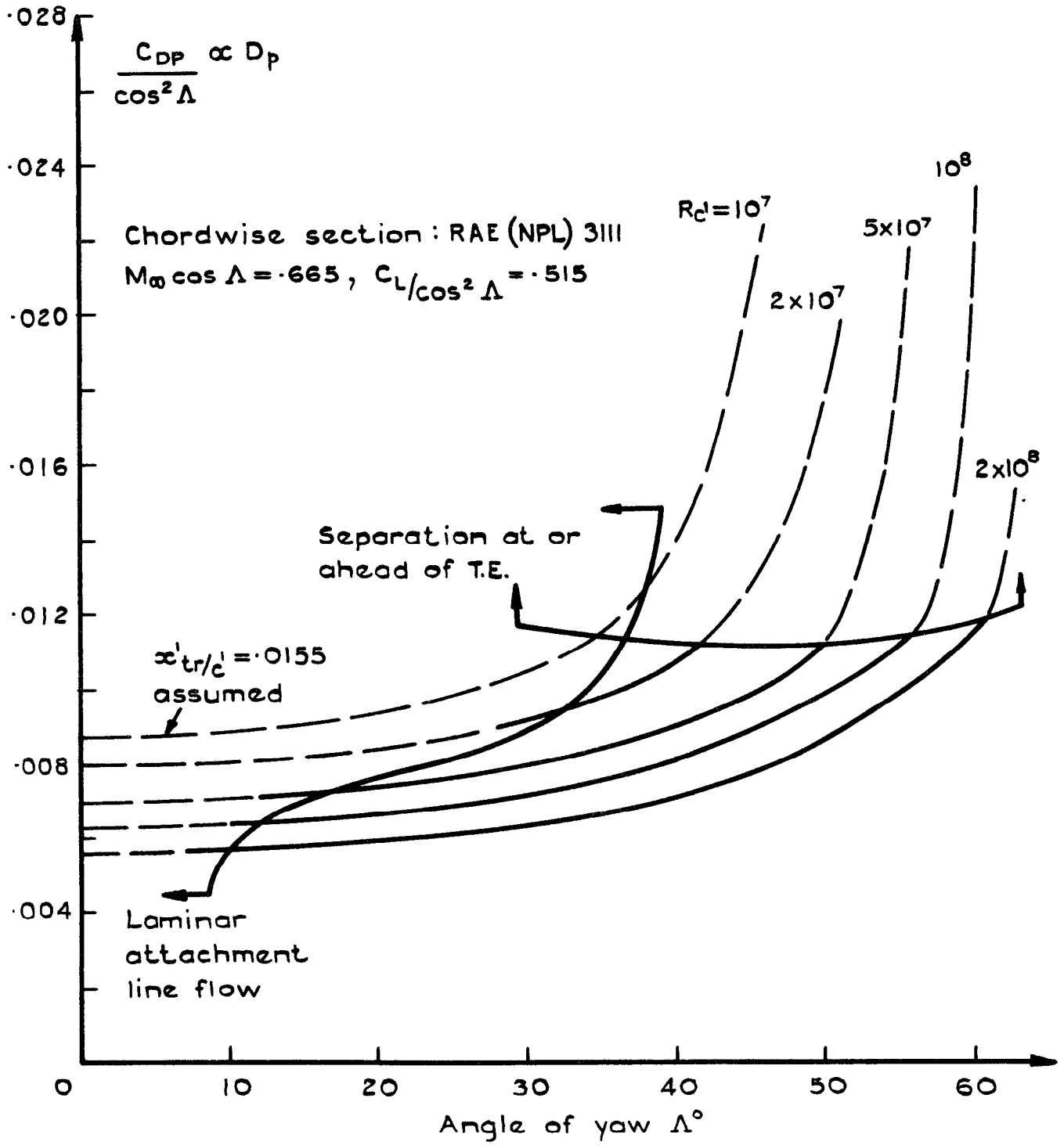

Fig.15 Variation of profile drag of a variable-sweep wing (see Fig 1b) operating at its section design point, at a given altitude and total aircraft weight

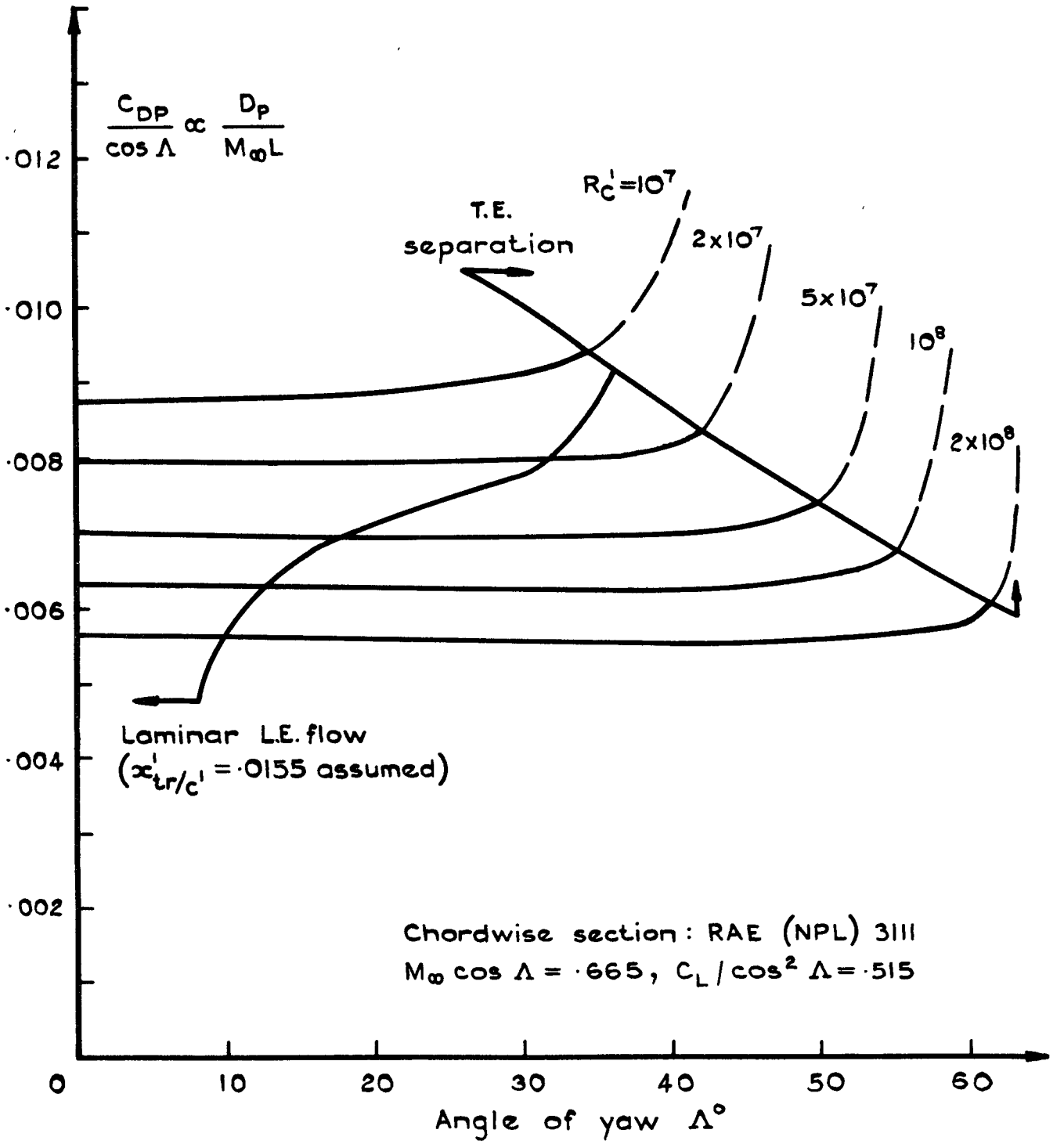

Fig.16 Variation of range parameter (based solely on profile drag) for the variable sweep wing, operating at its section design point

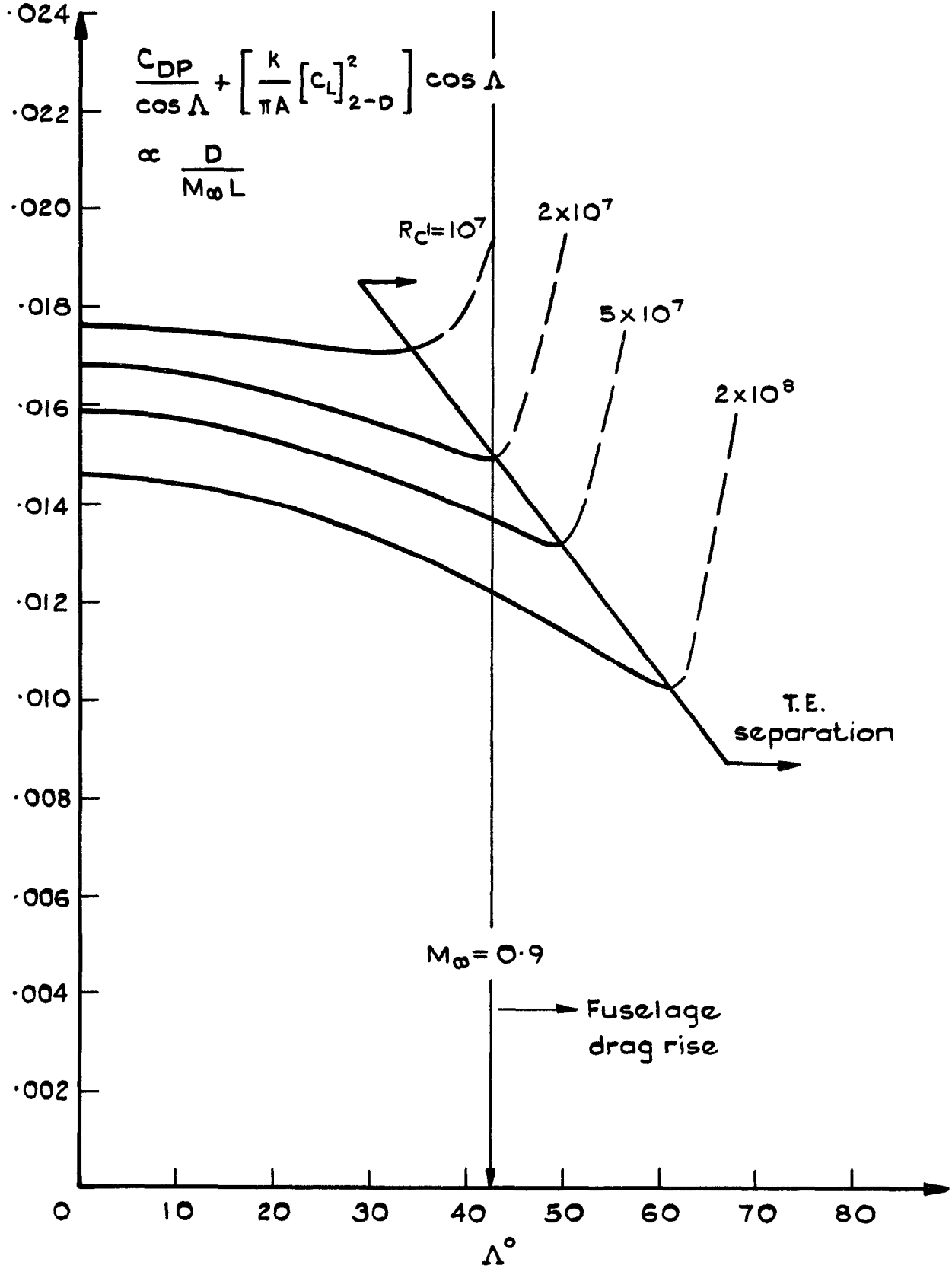

Fig.17 Effect of sweep on the range parameter (including vortex drag) for the variable sweep wing

Printed in England for Her Majesty's Stationery Office by the Royal Aircraft Establishment, Farnborough Dd 505376 K4 11/74

ARC CP No.1309
May 1973

Thompson, B. G. J.
Carr-Hill, G. A.
Ralph, M.

533.693.1 :
532.526 :
533.6.048.3 :
533.6.013.122 :
533.6.013.154

THE PREDICTION OF BOUNDARY-LAYER BEHAVIOUR AND PROFILE DRAG FOR INFINITE YAWED WINGS PART III CALCULATIONS FOR A PARTICULAR WING

An integral method is used to predict boundary-layer and wake behaviour for a family of infinite yawed wings having a chordwise section of NPL 3111 operating at its design sonic rooftop condition.

Profile drag predictions show a smaller variation with yaw than a typical project office design method. The Reynolds number for incipient rear separation depends strongly on angle of yaw. Scale effect on loss of lift, due to viscous displacement of the potential flow, appears to be amplified by sweep.

ARC CP No.1309
May 1973

Thompson, B. G. J.
Carr-Hill, G. A.
Ralph, M.

533.693.1 :
532.526 .
533.6.048.3
533.6.013.122 :
533.6.013.154

THE PREDICTION OF BOUNDARY-LAYER BEHAVIOUR AND PROFILE DRAG FOR INFINITE YAWED WINGS PART III CALCULATIONS FOR A PARTICULAR WING

An integral method is used to predict boundary-layer and wake behaviour for a family of infinite yawed wings having a chordwise section of NPL 3111 operating at its design sonic rooftop condition.

Profile drag predictions show a smaller variation with yaw than a typical project office design method. The Reynolds number for incipient rear separation depends strongly on angle of yaw. Scale effect on loss of lift, due to viscous displacement of the potential flow, appears to be amplified by sweep.

These abstract cards are inserted in Technical Reports for the convenience of Librarians and others who need to maintain an Information Index.

Cut here

ARC CP No.1309
May 1973

Thompson, B. G. J.
Carr-Hill, G. A.
Ralph, M.

533.693.1 :
532.526 .
533.6.048.3 :
533.6.013.122 :
533.6.013.154

THE PREDICTION OF BOUNDARY-LAYER BEHAVIOUR AND PROFILE DRAG FOR INFINITE YAWED WINGS PART III CALCULATIONS FOR A PARTICULAR WING

An integral method is used to predict boundary-layer and wake behaviour for a family of infinite yawed wings having a chordwise section of NPL 3111 operating at its design sonic rooftop condition.

Profile drag predictions show a smaller variation with yaw than a typical project office design method. The Reynolds number for incipient rear separation depends strongly on angle of yaw. Scale effect on loss of lift, due to viscous displacement of the potential flow, appears to be amplified by sweep.

ARC CP No.1309
May 1973

Thompson, B. G. J.
Carr-Hill, G. A.
Ralph, M.

533.693.1 :
532.526 :
533.6.048.3 :
533.6.013.122 :
533.6.013.154

THE PREDICTION OF BOUNDARY-LAYER BEHAVIOUR AND PROFILE DRAG FOR INFINITE YAWED WINGS PART III CALCULATIONS FOR A PARTICULAR WING

An integral method is used to predict boundary-layer and wake behaviour for a family of infinite yawed wings having a chordwise section of NPL 3111 operating at its design sonic rooftop condition.

Profile drag predictions show a smaller variation with yaw than a typical project office design method. The Reynolds number for incipient rear separation depends strongly on angle of yaw. Scale effect on loss of lift, due to viscous displacement of the potential flow, appears to be amplified by sweep.

Cut here

DETACHABLE ABSTRACT CARDS

DETACHABLE ABSTRACT CARDS

Published by
HER MAJESTY'S STATIONERY OFFICE

Government Bookshops
49 High Holborn, London WC1V 6HB
13a Castle Street, Edinburgh EH2 3AR
41 The Hayes, Cardiff CF1 1JW
Brazennose Street, Manchester M60 8AS
Southey House, Wine Street, Bristol BS1 2BQ
258 Broad Street, Birmingham B1 2HE
80 Chichester Street, Belfast BT1 4JY
Government Publications are also available through booksellers

C.P. No. 1309

ISBN 011 470893 2